Final Report

Sensitivity Analysis for Dynamic Failure and Damage in Metallic Structures

Office of Naval Research
800 North Quincy Street
Arlington, VA 22217-5000

Attention: Dr. Roshdy S. Barsoum

Submitted by:

Ahmed K. Noor
William E. Lobeck Professor of Aerospace Engineering
and
Director, Center for Advanced Engineering Environments

March 2005

School of Engineering and Technology
Old Dominion University
Norfolk, VA 23529

A final report submitted to the Office of Naval Research, Arlington, Virginia

REPORT DOCUMENTATION PAGE	Form Approved OMS No. 0704-0188

PLEASE DO NOT RETURN YOUR FORM TO THE ABOVE ADDRESS.

1. REPORT DATE *(DD-MM-YYYY)*	2. REPORT TYPE	3. DATES COVERED *(From - To)*
3-23-05	Final	2/1/01 – 3/31/05

4. TITLE AND SUBTITLE

Sensitivity Analysis for Dynamic Failure and Damage in Metallic Structures

5a. CONTRACT NUMBER

5b. GRANT NUMBER

N00014-01-1-0371

5c. PROGRAM ELEMENT NUMBER

6. AUTHOR(S)

Noor, Ahmed K.

5d. PROJECT NUMBER

5e. TASK NUMBER

5f. WORK UNIT NUMBER

7. PERFORMING ORGANIZATION NAME(S).AND ADDRESS(ES)

Old Dominion University
Center for Advanced Engineering Environments
600 Butler Farm Road, Suite 200
Hampton, VA 23666

8. PERFORMING ORGANIZATION REPORT NUMBER

ODU Research Foundation
Project #212151

9. SPONSORING/MONITORING AGENCY NAME(S) AND ADDRESS(ES)

Department of the Navy, Office of Naval Research
800 North Quincy Street
Arlington, VA 22217-5660

10. SPONSOR/MONITOR'S ACRONYM(S)

11. SPONSOR/MONITOR'S REPORT NUMBER(S)

12. DISTRIBUTION/AVAILABILITY STATEMENT

Publically available

13. SUPPLEMENTARY NOTES

14. ABSTRACT

The objective of the study conducted under this grant is to develop effective computational strategies for: a) assessing the sensitivity of the dynamic failure and damage of metallic structures to variations in both the microstructure and macrostructure material parameters; and b) incorporating the uncertainties in material parameters in the prediction of response and damage of these structures. The sensitivity coefficients, which are the derivatives of the various structural response quantities with respect to the material parameters, are evaluated by using the direct differentiation method.

15. SUBJECT TERMS

sensitivity analysis, dynamic failure, metallic structures, microstructure solidification, welding residual stresses, thermo-elasto-plastic, interrogative visualization

16. SECURITY CLASSIFICATION OF:			17. LIMITATION OF ABSTRACT	18. NUMBER OF PAGES	19a. NAME OF RESPONSIBLE PERSON
a. REPORT	b.ABSTRACT	c. THIS PAGE			Ahmed K. Noor
U	U	U	UU	1	19b. TELEPHONE NUMBER *(Include area code)* 757-766-5233

Title: Sensitivity Analysis for Dynamic Failure and Damage in Metallic Structures

Date Submitted: March 21, 2005

1. Principal Investigator/

Technical Contact:

Ahmed K. Noor
Center for Advanced Engineering Environments
School of Engineering and Technology
600 Butler Farm Road
Suite 200
Hampton, VA 23666
Phone (757) 766-5233; Fax (757) 766-5246
Email: a.k.noor@larc.nasa.gov

Duration: Feb. 1, 2001-March 2005

Old Dominion University is an educational institution participating in the Federal Demonstration Project.

Table of Contents **Page**

Abstract

The objective of the study conducted under this grant is to develop effective computational strategies for: a) assessing the sensitivity of the dynamic failure and damage of metallic structures to variations in both the microstructure and macrostructure material parameters; and b) incorporating the uncertainties in material parameters in the prediction of response and damage of these structures. The sensitivity coefficients, which are the derivatives of the various structural response quantities with respect to the material parameters, are evaluated by using the direct differentiation method.

A two-phase computational procedure is applied to the uncertainty analysis of dynamic failure in metallic structures. In the first phase the sensitivity analysis is used to identify the major material parameters, i.e., the parameters which have the most impact on the response and failure. In the second phase, the major parameters are treated as fuzzy parameters, and the fuzzy set techniques are used to provide information about the range and variation of possible response quantities and damage associated with pre-selected ranges and variations of the major parameter.

The computational procedure developed under this grant can be used to generate a toolkit of the uncertainty analysis procedure that allows commercial deterministic analysis codes to perform uncertainty analysis. This is accomplished by modifying the input (to include the pre-selected variations in the major parameters), and adding a postprocessor to generate the range of variation of different response quantities.

A number of thermo-viscoplastic material models will be developed to study the effect of rate-sensitivity on welding residual stresses in stainless steel AL6XN. Also, material models are developed which reduce to viscous models above the solidus temperature Ts and to rate independent plastic models below 0.4 Ts. Between those two temperature ranges, the models describe rate-dependent plastic behavior. Attempt was made to estimate the values of the material parameters, over wide ranges of temperatures and strain rates, by working closely with researchers performing experiments. A number of arc and laser welding techniques for residual stress mitigation are considered. The effect of variation in material parameters, which have the most impact on the response and damage, are studied by using fuzzy-set techniques.

1. Background and Brief Overview of Previous Work

The formation of residual stresses is inevitable in any welding operation. When combined with the externally applied stress fields, the residual stresses can result in significant differences in the performance of welded structures such as dimensional stability, fatigue strength, and resistance to environmentally induced cracking [Ref. 1]. Furthermore, it has been shown [e.g., Refs. 2, 3] that the residual stresses can significantly affect the fracture behavior of welded components.

The formation of welding residual stress in engineering materials is a complex thermal-mechanical-metallurgical process. A welding operation introduces localized heating and cooling around the joint region. Material expands on heating and contracts on cooling. The localized material expansion and contraction during welding create a transient, non-uniform deformation process which results in the formation of residual stresses due to the uneven distribution of the inelastic strains. For many engineering alloys, the welding thermal cycle would induce metallurgical changes in the heat affected zone (HAZ) and the weld metal. These microstructural changes could have profound influence on the distribution of residual stresses in the weldment, due to the formation of complex material property gradients, the transformation-induced plasticity, and the specific volume changes of the microstructure constituents associated with the phase transformations in the HAZ and weld metal. The thermal-mechanical-metallurgical interactions of a material during welding and their effects on residual stresses are illustrated in Figure 1.

As shown in Figure 1, the material to be welded and the welding process conditions are two primary factors governing the formation of residual stresses of a weldment.

The welding induced residual stresses strongly depend on the material to be welded. Both the thermophysical properties and the mechanical properties of a material would influence the residual stresses in a welded structure. The thermophysical properties (thermal conductivity, specific heat, latent heat of fusion, and density) influence the temperature field surrounding the weld pool, thereby influencing the thermal expansion and contraction behaviors of the material during welding. The mechanical properties (elastic modulus, yield strength, flow stress, and thermal expansion coefficient) contribute directly to the stress evolution during a welding cycle. The microstructural and associate metallurgical changes contribute property changes in the weld region are highly dependent on the type of alloy system and the composition of alloys.

The weld residual stresses also strongly depend on welding process conditions. Fundamentally, it is the thermal energy from a welding heat source that drives the heat flow in the material being welded. The spatial and temporal distributions of the welding temperature field is directly related to the welding process conditions such as welding speed, and the intensity and distribution of the heat input. Changes in the temperature field not only alter the thermal expansion and contraction process, but also the phase transformation behaviors of the material during welding; both would influence the residual stresses and distortions of welded structures.

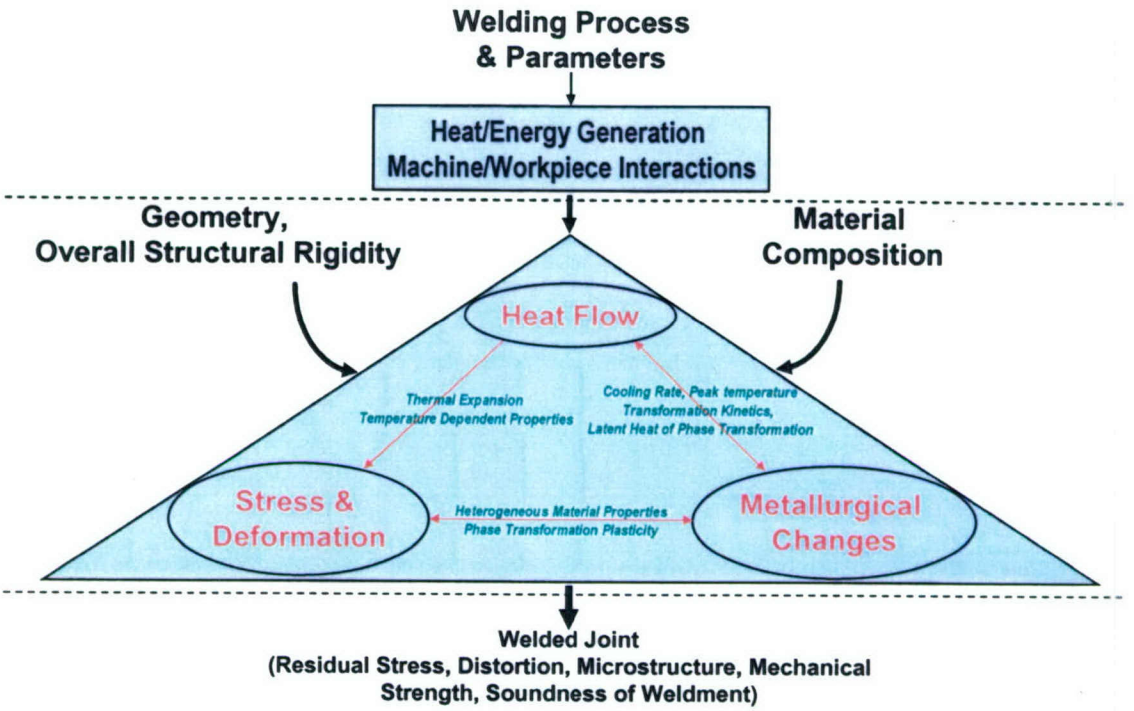

Figure 1 Primary factors and the thermal-mechanical-metallurgical interactions during welding that contribute to the formation of weld residual stresses and performance of welded structures.

Understanding the effects of welding process conditions on weld residual stresses is not only a fundamental subject of welding science, but also has broad practical implications. For many Navy applications, the selection of materials and the design of a welded structure are often determined based on the overall performance requirements of the structure; they are seldom changeable because of welding related considerations. Thus, from a practical point of view, effective control and mitigation of weld residual stresses and distortions would mainly rely on proper selection of welding process conditions. Over the years, the welding community has considered many welding and post-welding techniques to manage the residual stresses and distortions [Ref. 1]. However, much of the development has been based on the time-consuming and costly trial-and-error experimental testing, and often with limited success.

In recent years, there have been attempts to "pro-actively" manage the thermomechanical deformation process during welding to control the welding residual stresses and distortions. Among the proposed approaches are the so-called low-stress and no-distortion welding for thin structure panels [Ref. 4], the thermal tensioning welding (a derivative of the no-distortion and low-stress technique) for shipyard panels [Ref. 5], the active quenching welding [Ref. 6], and the use of low-temperature phase transformation filler metal in welding [Ref. 7]. Although limited success have been reported of these techniques, they are still in the early stages of research and development – the process window in which each of the aforementioned techniques operates is generally not well defined in terms of the key process conditions and structural geometry.

Clearly, understanding the sensitivity of thermal-mechanical-metallurgical responses of material to variations in welding process conditions would be a critical aspect toward widespread applications of the above welding techniques to mitigate the welding residual stresses and minimize their detrimental effects. Built upon the progress of the current ONR grant, the focus of future research should be on investigating the effects of the welding process conditions.

The study under this ONR grant, focused on the development of an integrated computational welding simulation environment that can be used to systematically investigate and interrogate the sensitivity and variability of the thermal-mechanical-metallurgical responses of welded components to various material, geometric and welding conditions. The computational simulation environment consists of (1) advanced welding simulation procedures, (2) effective sensitivity and fuzzy-set analysis methodology, and (3) advanced computer visualization technology to investigate and interrogate the sensitivity and variability of the response to variations in material parameters.

The advanced welding simulation procedure integrated the metallurgical and microstructural computation algorithms into finite element based thermo-mechanical code. This allows for fundamental investigation of the effects of material properties variations/gradients in the weld joint region on the performance of welded metallic structures.

The framework of the computational welding simulation environment was developed and applied to investigate the effect of uncertainties in material properties.

2. Mathematical Formulation

This section describes the basic mathematical formulations of the thermal-mechanical deformation process during welding, focusing on the formulations of the stress-strain constitutive relation as function of temperature and the phase transformation processes. These formulations are essential to the sensitivity study of the welding process effects. The mathematical formulations and numerical implementation of other aspects of thermal-mechanical-metallurgical simulation of welding process can be found in the literature [for example, Refs. 8-103. The treatments of the sensitivity and fuzzy-set analysis can also be found in Refs 14 to 16.

Uncoupled thermomechanical analysis is performed. The temperature field is assumed to be independent of stress and strains. The governing equations for the thermal and mechanical analysis are summarized subsequently.

2.1 Thermal Analysis

2.1.1 Governing equations

The heat flow during arc welding was modeled as a heat condition formulation. The convective heat transfer inside the weld pool due to circulation of the molten metal was not

explicitly simulated, but the convective effect was accounted for in the heat conduction model by means of effective thermal properties such as effective thermal conductivity. The governing equation for transient heat conduction analysis is given by:

$$\nabla \cdot (\kappa \nabla T(r,t)) + Q = \rho C_p \frac{dT(r,t)}{dt} \tag{1}$$

where ρ is the density of the material, *Cp* the specific heat, κ the thermal conductivity, *Q* the internal heat generation rate, and *T* the temperature. *r* is the coordinate of the material, *t* is the time.

2.1.2 Boundary conditions

The heat from the welding arc was treated as a volumetric heat source, taking the ellipsoidal distribution proposed by Goldak et al. [11].

$$q = \frac{6\sqrt{3}\eta EI}{\pi\sqrt{\pi}abc} e^{\left[-3\left(\frac{x^2}{a^2}+\frac{y^2}{b^2}+\frac{z^2}{c^2}\right)\right]} \tag{2}$$

where q is the energy density (W/mm^3) from the weld arc, η is the arc efficiency. For the FCAW process used to weld the gussets, an arc efficiency value of 0.8 was used. E and I are the welding voltage and current, respectively. The parameters *a, b, c* are related to characteristics of the electrode, and represent the arc energy distribution profile of the FCAW process. The origin of the *(x, y, z)* coordinate system is fixed at the center of the weld arc.

For the cross-section model used in this study, the welding heat is effectively applied simultaneously over the weld length. This necessitates the following transformation of the Goldak model:

$$q = \frac{6\sqrt{3}\eta EI}{\pi\sqrt{\pi}abc} e^{\left[-3\left(\frac{(\chi-\chi_0)^2}{a^2}+\frac{(\varsigma-\varsigma_0)^2}{b^2}+\frac{(V(t-t_o))^2}{c^2}\right)\right]} \tag{3}$$

where t is the heating time, and V is the arc travel speed. The heat input is expressed in the local coordinate system (χ, ξ) associated with individual weld pass as shown in Figure 2. The center of the welding arc is located at (χ_o, ξ_o). t_o is selected such that, at $t=0$, the arc exerts negligible heating at the modeling plane. The heating then increases as the analysis proceeds, and reaches the peak value at $t=t_o$. The heat input in Equation (2) was programmed via the DFLUX user subroutine interface in ABAQUS.

For all exposed surface of the model, both convection heat loss and radiation heat loss were considered:

$$q_{loss} = -h(T - T_\infty) - \sigma\varepsilon(T^4 - T_\infty^4) \tag{4}$$

where h is convection heat loss coefficient, ε the radiative emissivity, and σ the Stefan-Boltzman constant.

2.1.3 Solidification model

Under the welding conditions characteristic to this study, the nonequilibrium solidification process results in formation of dendrite microstructure in the weld pool (constitutional super-cooling) [12]. The release of the latent heat of fusion during melting and solidification can greatly affect the shape and size, and thermal stresses around the weld pool. Since the present work is concerned with the temperature around the weld pool, it is important to have a more realistic model for the release rate of latent heat in order to better simulate the temperature distribution. In this study, the release of latent heat of fusion is related to the microscopic kinetics of the solidification process in the weld pool.

The release of latent heat during solidification is treated as an internal heat generation term in the heat flow in the governing equation for heat transfer:

$$Q = \begin{cases} q_i & for \quad T_s < T < T_L \\ 0 & for \quad T_s > T, or\ T > T_L \end{cases} \tag{5}$$

where q is the release rate of latent heat of fusion, and Ts and T_L are the solidus and liquidus temperature of the alloy.

The rate of latent heat release is assumed to be proportional to the rate of solid fraction change in the solidification temperature range and can be written as:

$$q_i = L\frac{df_s}{dt} \tag{6}$$

where L is the volumetric latent heat of fusion (J/mm^3).

For substitutional alloying elements, the Scheil equation can be used to describe the fraction of solid as a function of the solid composition at the solid-liquid interface:

$$C_s^* = kC_0(1-f_s)^{(k-1)} \tag{7}$$

DuPont [13] developed a pseudo Fe-Mo binary phase diagram for AL-6XN, in which the solid interface composition is related to the temperature at the solid-liquid interface. Taking advantage of this relation, the rate of latent heat release can be written as:

$$q_i = L\frac{df_s}{dt} = L\frac{df_s}{dC_s^*}\frac{dC_s^*}{dT}\frac{dT}{dt}$$

$$= \frac{L(kC_o)^{\frac{1}{1-k}}}{m_s(1-k)}\left[\frac{T-T_s}{m_s} + C_{SE}\right]^{\frac{2-k}{k-1}} \cdot \frac{dT}{dt}$$

All the material parameters in the above equation are given in Table 1.

2.2 Mechanical Analysis

The welding thermal cycle causes metallurgical transformations to take place in many high-performance engineering alloys of interest to the Navy. Those transformations occur on the microstructural level (grain length scale) and manifest themselves macroscopically in the form of latent heat generation as well as additional dilatational and deviatoric deformations. The latent heat affects temperature history during welding and, hence, indirectly affects the residual stresses.

Therefore, in addition to the elastic, plastic and thermal strains in a classical thermomechanical deformation problem, the solid-state phase transformations during welding give rise to two additional strains. The total strain rate can, therefore, be decomposed into five components as follows (Ref. 17):

$$\dot{\boldsymbol{\varepsilon}} = \dot{\boldsymbol{\varepsilon}}^{e} + \dot{\boldsymbol{\varepsilon}}^{p} + \dot{\boldsymbol{\varepsilon}}^{th} + \dot{\boldsymbol{\varepsilon}}^{tr} + \dot{\boldsymbol{\varepsilon}}^{tp} \tag{8}$$

The components on the right-hand side of Eq. (8) correspond to elastic, plastic, thermal, transformation, and transformation plasticity strain rates, respectively. In Eq. (8), as well as in the sequel, boldface letters and symbols refer to second order tensors. It has been shown [see, for instance, Refs. 18, 19] that the strain components ε^{tr} and ε^{tp} have a major effect on the welding residual stress fields and, therefore, should be accounted for in any reliable analysis of those fields.

The elastic strain is modeled using the isotropic Hooke's law with temperature-dependent Young's modulus and Poisson's ratio. For the plastic strain component a rate-independent plastic model is employed with the following features: kinematic hardening, the von Mises yield surface, and temperature-dependent material properties. Kinematic hardening is considered a significant feature since material points typically undergo both loading and unloading during the weld thermal cycle [Ref. 20]. Denoting the back stress tensor by α and the yield function by ϕ, the plastic strain can be expressed in the form:

$$\dot{\boldsymbol{\varepsilon}}^{p} = \dot{\varepsilon}^{p} \frac{\partial \phi(\sigma - \alpha)}{\partial \sigma} \tag{9}$$

where

$$\phi = \sqrt{\frac{3}{2}(\sigma' - \alpha') \bullet (\sigma' - \alpha')} - \sigma_0 = 0 \tag{10}$$

In Eq.11, $\dot{\varepsilon}^{p}$ is the equivalent plastic strain rate:

$$\dot{\varepsilon}^{p} = \sqrt{\frac{3}{2}\, \dot{\boldsymbol{\varepsilon}}^{p} \bullet \dot{\boldsymbol{\varepsilon}}^{p}} \tag{13}$$

In Eq. (10), σ_0 is the initial yield stress surface which depends on both temperature and microstructure constituents, $(\,)\bullet(\,)$ indicates inner product of two tensors, σ' is the deviatoric stress tensor:

$$\sigma' = \sigma - \sigma_h \mathrm{I}; \quad \sigma_h = \frac{1}{3}\mathrm{tr}\ \sigma \tag{14}$$

where σ_h is the hydrostatic stress, I is the second-order identity tensor, and tr denotes the trace of a tensor. Similarly, in Eq. (10), α' is the deviatoric part of α. At high temperatures the stress-strain curves typically exhibit pronounced curvatures and, therefore, a nonlinear kinematic hardening rule is used to describe the evolution of α. The rule is based on the work of Lemaitre and Chaboche [Ref. 14] and reads:

$$\dot{\alpha} = H\dot{\varepsilon}^{p}\frac{(\sigma-\alpha)}{\sigma_0} - \gamma\dot{\varepsilon}^{p}\alpha + \frac{1}{H}\frac{dH}{dT}\dot{T}\alpha \tag{15}$$

where H is a temperature and microstructure dependent hardening coefficient and γ is a recovery coefficient.

The thermal strain rate component is given by the relation:

$$\dot{\varepsilon}^{th} = \alpha_T(T,\xi_A,\xi_M,\xi_L)\dot{T}\mathrm{I} \tag{16}$$

where α_T is the coefficient of thermal expansion (CTE) which depends on temperature as well as the different phases present. The latter dependence is modeled using the linear rule of mixtures. The CTE of the liquid phase is taken to be zero to suppress the thermal expansion at temperatures above the melting point.

The transformation strain ε^{tr} is purely dilatational and results from contraction and expansion of the material during allotropic phase transformations (such as formation of the austenite on heating and decomposition of the austenite on cooling of ferritic alloy steels). This strain component can be expressed mathematically by the following simple empirical form [Ref. 17]:

$$\dot{\varepsilon}^{tr} = \eta\ \dot{\xi}\mathrm{I} \tag{17}$$

In Eq. (17), η is a material parameter whose value can be determined from the total material contraction and expansion induced by the transformation and obtained from dilatometer measurements. $\dot{\xi}$ is the transformation rate $\left(\dot{\xi} = \dot{\xi}_A \text{ or } \dot{\xi}_M\right)$.

The strain component ε^{tr} is deviatoric and is linearly proportional to the stress. It occurs only during the period of martensitic transformation, and is irrecoverable upon removal of the stress. This component can be expressed using the following empirical relation (Ref.).

$$\dot{\varepsilon}^{tp} = \frac{3}{2}\lambda(1-\xi_M)\dot{\xi}_M\ \sigma' \tag{18}$$

where λ is a material parameter.

As shown above, the effects of metallurgical transformations manifest in two ways – the additional two strain components in Eq. (8), and the dependency of the yield stress surface on the microstructure constituents present at the material point in Eq. (10) and (15).

3. Finite Element Discretization

The heat transfer equations emanating from a finite-element semi-discretization are integrated using an implicit backward difference scheme to generate the time history of the temperatures. The mechanical response during welding is them calculated by using a rate-independent, small deformation thermo-elasto-plastic material molded with temperature-dependent material properties.

4. Sensitivity Analysis

The sensitivity coefficients, which are the derivatives of the various thermal and mechanical response quantities with respect to the material parameters, are evaluated buy using the direct differentiation method in conjunction with the automatic differentiation software facility ADIFOR. The sensitivity coefficients obtained by ADIFOR were validated by comparing them with those obtained by finite difference approximations, using different finite difference intervals.

5. Numerical Studies

A number of studies have been reported for the temperature, residual stress-time histories and their sensitivity coefficients for a double fillet conventional welding of a stiffener and a base plate made of stainless AL-6XN (Ref. 16). Herein, the sensitivity of the temperature with respect to microstructural parameters is presented.

5.1 Material, Geometry and Welding conditions

Alloy AL-6XN, a super austenitic stainless steel, was used in this study. It was chosen because microsegregation and solidification cracking have been two major concerns in welding AL-6XN [12]. Table 2 shows the nominal composition of AL-6XN used in the study. It is noted that the alloy consists of mostly substitution alloying elements, thereby the Scheil equation, would be adequate to treat the micro-segregation and release of the latent heat of fusion during solidification.

The weld joint geometry used in this study is a double fillet Tee-Joint, representing a stiffened structure panel commonly used for Navy ship structure constructions. The dimensions

of the weld joint are given in Figure 2. The bottom panel plate was 20-in long, 20-in wide, whereas the vertical stiffener was 8-in high. Both the panel plate and the stiffener were ½-in thick. The selection of this particular panel configuration was consistent with previous studies sponsored by US Navy on ship panel structures [21,22]. All welding conditions used in this study were also based on the previous experimental welding tests. They are summarized below.

The stiffened thin-section panel was welded using flux cored arc welding (FCAW) process. The double-fillet welds were made with twin-torch configuration: two weld torches were used to simultaneously deposit the two weld beads on two sides of the stiffener. The twin-touch arrangement is commonly used in the shipyard to increase the productivity and to maintain symmetry about the stiffener for distortion control. The baseline welding parameters included the followings: welding voltage – 24V, welding current – 245A, and welding travel speed – 14 in/min. The two welding guns were arranged such that the second welding gun was trailing the first one by 3.5 in during welding. The nominal fillet size was ¼ in wide and ¼-in high. The stiffener was tack-welded to the panel at both ends before the fillet welds were made.

5.2 Finite element model

The two-dimensional cross-section model was used for studying the effect of alloy composition variations on the temperature field during the weld metal solidification. In order to appropriately simulate the release of latent heat during solidification based on the solidification kinetics discussed in Section, the element size in the weld region needs to be in the range of 0.1 to 0.2 mm. A full 3-dimensional model with such small elements would be too large to solve practically with the computational power available to the program.

Because of its computational efficiency, a two-dimensional cross-section model was used. This model utilized only a cross-sectional plane, perpendicular to the weld length, of the T-joint structure in the analysis. The appropriate use of the cross-sectional model for long, straight welds such as those of this study has been well documented in many studies in the past. The cross-sectional model is generally accurate when the quasi-steady state is established in the middle portion of the welded structure, thereby adequate for comparative evaluations of the alloy composition variations in this study.

The 2-dimensional cross-section model consists of approximately 8600 element. The T-joint was discretized with 4-noded quadrilateral linear isoparametric elements. The linear element is more suitable for handling the latent heat effects associated with welding solidification [23]. Figure 4 shows the finite element mesh around the double-fillet welds of the 2-dimensional model.

For evaluation of the sensitivity of mechanical properties and welding process parameters, a full 3-dimensional model was used. The T-joint was discretized with 8-noded linear isoparametric elements. The element size in the weld region was about 1-mm. The entire stiffened panel consisted of approximately 74,000 elements and 90,000 nodes.

The calculations were carried out with the general-purpose code ABAQUS (Version 6.3) [24], enhanced with a set of proprietary user subroutines to deal with the special issues associated with welding process simulations that have been described in the previous sections.

5.3 Selection of material parameters and their variation ranges

This study focused on the sensitivity study of the material parameters mostly affecting the solidification kinetics during welding. The parameters consisted of the thermophysical properties and the solidification parameters as defined in Table . Their effects on the temperature near the solidification temperature range were analyzed.

The thermophysical properties (thermal conductivity, specific heat) were temperature dependent and were taken from a recent study by Nied et al [25]. They are provided in Figure 6. The thermal conductivity above the melting temperature is artificially increased to compensate for the convection heat transfer effect in the molten weld pool.

For the sensitivity analysis, variations of the above thermophysical properties at 1600K (near the nominal solidus temperature of AL-6XN) was made at ±0.1%, 0.5% and 1% to study their effects on the temperature field in the solidification temperature range. The solidification parameters in Table were also symmetrically varied at ±0.01%, 0.05%, 0.1%, and 0.5%.

6. Results and Discussions

After the welding heat flow analyses were performed using the finite element model, the thermal histories at eight points near the weld joint were chosen to perform the sensitivity analysis to assess the effects of various material parameters on the transient temperature distribution around the molten weld pool. These eight points are identified in Figure 7. Figure 7 shows the typical thermal histories at four points on the right weld (Points 5 to 8 in Figure 6). There are noticeable second, lower peak in the plots, associated with the heating from the trailing welding arc on the other side of the web plate. Also noticeable in the plot was the drastic change in the cooling rate at the center point of the weld surface (Point 6) due to the release of the latent heat as the weld is solidified.

The finite difference sensitivity analysis showed very good convergence, with decreasing the finite difference interval, for all the material parameters studied here. As an example, Figure 9 compares the calculated normalized sensitivity of temperature with respect to the nominal alloy composition for four different finite difference intervals (0.01%, 0.05%, 0.1%, and 0.5%) at the center point of weld surface (Point 6 in Figure 7). Very good convergence was obtained for the entire welding time considered. It is also important to notice that the maximum sensitivity occurred when the temperature was high, suggesting that the variations in solidification parameters has the greatest influence in the solidification temperature range that is critical to the formation of weld defects.

7. Proposed Future Work

Based on the present study, future work should focus on investigating the effects of welding process conditions on the microstructural variations and residual stresses of welded structures, by utilizing the computational welding simulation environment developed in the present ONR study. The porposed research and development activities include the following major efforts:

(1) Refine the microstructural models to cover both diffusive and non-diffusive phase transformation mechanisms, and integrate these microstructural models into the computational welding simulation environment.
(2) Establish an effective computational methodology for sensitivity analysis of the residual stresses to variations of various welding process conditions. Well-established methods in probability theory can be used to characterize uncertainty in process conditions. However, for situations where the uncertainty is of a non-stochastic nature (e.g., uncertainty arising from imprecision or fuzziness), the fuzzy set approach has been suggested to be more appropriate for modeling uncertainty.
(3) Study the sensitivity of key welding process parameters in several promising welding techniques for residual stress mitigation such as active quenching, low temperature phase transformation filler metal, and low-stress and no-distortion welding. Both arc welding and laser welding will be studied.
(4) Incorporate the local microstructure and property gradients in the HAZ and weld region into dynamic failure and damage analysis of metallic structures.

The proposed uncertainty analysis will provide upper and lower bounds (i.e., envelopes) for the welding residual stresses and distortions as functions of the variability in welding process conditions. These bounds can help achieve the following:

- Better understanding of the mechanical response, fracture behavior, and failure of welded structural components;
- Better fitness-for-purpose assessments of welded structural components; and
- Optimization of the weld process selection and control to reduce the residual stresses.

8. References

1 American Welding Society, *Welding Handbook*, 9th edition. 2001.

2 Panontin, T. L. and Hill, M. R., "The Effect of Residual Stresses on Brittle and Ductile Fracture Initiation Predicted by Micromechanical Models," *International Journal of Fracture*, Vol. 82, 1996, pp. 317-333.

3 Masubuchi, K., *Analysis of Welded Structures*, Pergamon Press, 1980.

4 Guan, Q. "Efforts to eliminating welding buckling distortions - from passive measures to active in-process control," *Today and Tomorrow in Science and Technology of Welding and Joining*, 7th JWS International Symposium, Kobe, 20-22 Nov.2001

5 Deo, M.V., Michaleris, P. "Mitigation of welding induced buckling distortion using transient thermal tensioning," *Science and Technology of Welding and Joining*, v8, 2003. pp. 49-54.

6 Feng, Z., White, R.A., Willis, E., and Solomon, H.D., 1999, "Development of compressive residual stresses in underwater PTA welds," *9th Int. Conf. On Environmental Degradation of Materials in Nuclear Power Systems Water Reactors*, TMS, 757-764.

7 Zenitani, S. et al., "Prevention of Cold Cracking in High-Strength Steel Welds by Applying Newly Developed Low Transformation-Temperature Welding Consumables," *Proc. 6th Int. Trends in Welding Research*, 2002, ASM International, pp. 569-574.

8 H.D. Hibbitt, and P.V. Marcal, "A Numerical, Thermo-Mechanical Model for the Welding and Subsequent Loading of a Fabricated Structure," *Computers & Structures*, Vol.3, 1145-1174, 1973.

9 Goldak, J, Chakravarti, A, and Bibby, M. "A New Finite Element Model for Welding Heat Sources," *Metall. Trans.* Vol. 15B, 299-305, 1984.
10 Z. Feng, "A Computational Analysis of Thermal and Mechanical Conditions for Weld Metal Solidification Cracking," *Welding in the World*, 33(5): 340-347, 1994.
11 J. Goldak, A. Chakravarti and M. Bibby, "A New Finite Element Model for Welding Heat Sources," *Metall. Trans.* Vol. 15B, 299-305, 1984.
12 J.N. DuPont, *Welding J.* 2000, **78**, 253s-263s.
13 J.N. DuPont, Private communication, 2003.
14 Abdel-Tawab, K. and Noor, A.K., "A Fuzzy-set Analysis for a Dynamic Thermo-elasto-viscoplastic Damage Response," *Computers and Structures*, Vol. 70, 1999, pp. 91-107.
15 Abdel-Tawab, K. and Noor, A.K., "Uncertainty Analysis of Welding Residual Stress Fields," *Computer Methods in Applied Mechanics and Engineering*, Vol. 179, 1999, pp. 327-344.
16 Song, J., Peters, J., Noor, A. and Michaleris, P., "Sensitivity Analysis of the Thermomechanical Response of Welded Joints," *International Journal of Solids and Structures*, Vol. 40, 2003, pp. 4167-4180.
17 Radaj, D., *Heat Effects of Welding*, Springer-Verlag, New York, 1992.
18 Oddy, A.S., Goldak, J.A. and McDill, J.M.J., "Transformation Plasticity and Residual Stresses in Single-Pass Repair Welds," *Journal of Pressure Vessel Technology*, Vol. 114, 1992, pp. 33-38.
19 Lemaitre, J. and Chaboche, J.-L., *Mechanics of Solid Materials*, Cambridge University Press, New York, 1990.
20 Denis, S. Gautier, E., Simon, A. and Beck, G., "Stress-Phase-Transformation Interactions-Basic Principles, Modeling and Calculation of Internal Stresses," *Material Science and Technology*, Vol. 1, 1985, pp. 805-814.

9. Publications and Presentations

The list of journal articles authored by the principal investigator and his coworkers I the results of the ONR grant is given in Appendix I. Abstracts of the articles are given in Appendix II. Screenshots of a detailed presentation on residual stresses and distortions in large welded structures are given in Appendix III.

Table 1 Material parameters used in this study (After DuPont [13])

Parameters	Symbol, unit	Value
Nominal Alloy Composition	C_0, Wt-%	6.3
Maximum solid solubility	C_{SE}, Wt-%	9.4
Solute partition ratio (dendrite core / nominal alloy composition)	κ	0.66

Solidus slope	m_s, K/Wt-%	-17
Melting Temperature	To, °C	1490
Density	ρ, g/mm^3	8.06 x 10^{-3}
Volumetric Latent Heat of Fusion	L, J/mm^3	2.1

Table 2 Nominal composition of AL-6XN, in wt-%.

Fe	Ni	Cr	Mo	Other
47	24.4	20.9	6.3	0.9

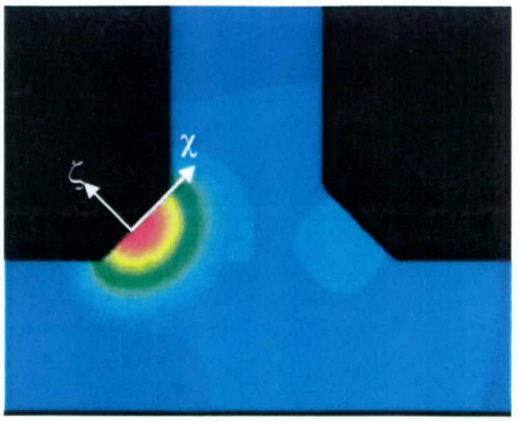

Figure 2 Local coordinate system used to define the welding heat input.

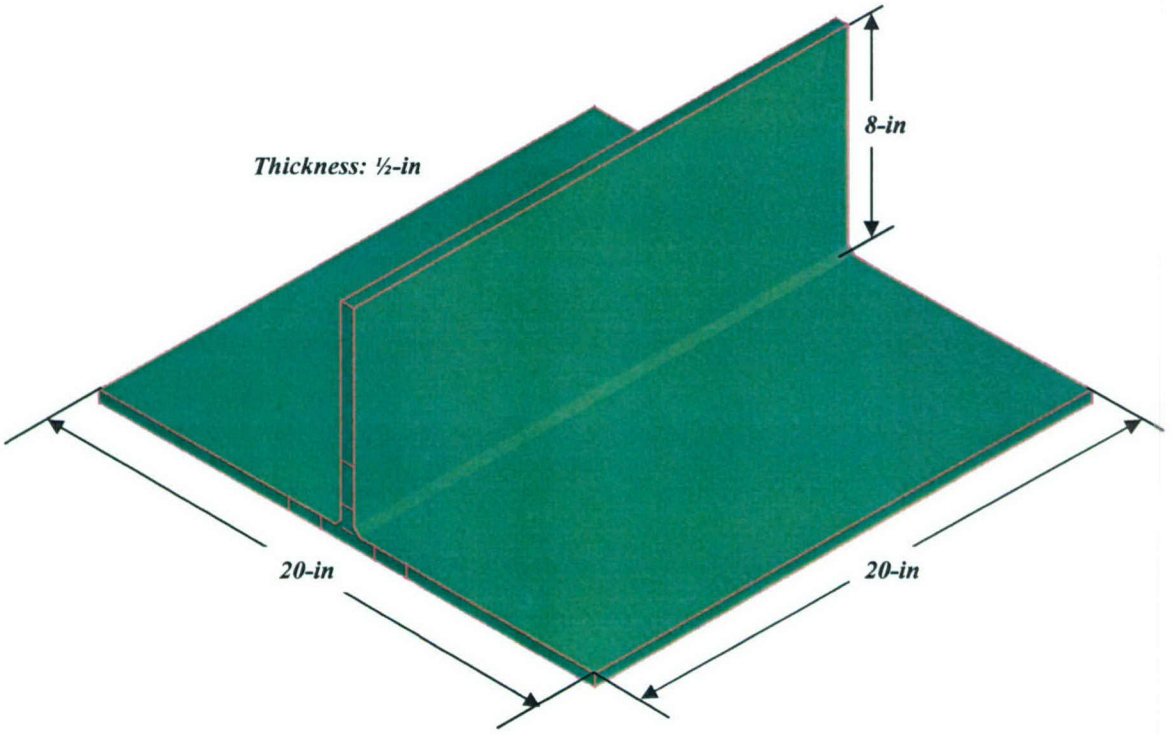

Figure 3 Dimensions of the T-joint used in this study

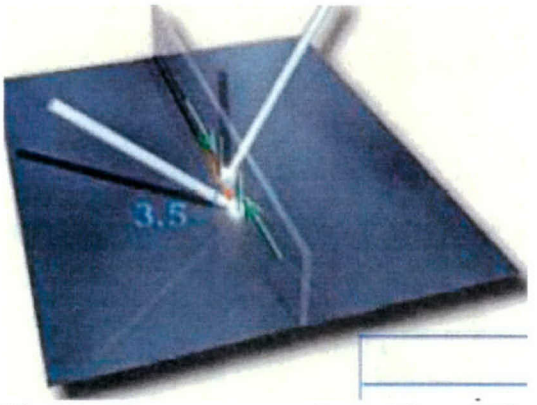

Figure 4 The twin-welding torch arrangement used in making the two fillet welds on the T-joint. The welding torch on the left side follows the right side torch by 3.5 in.

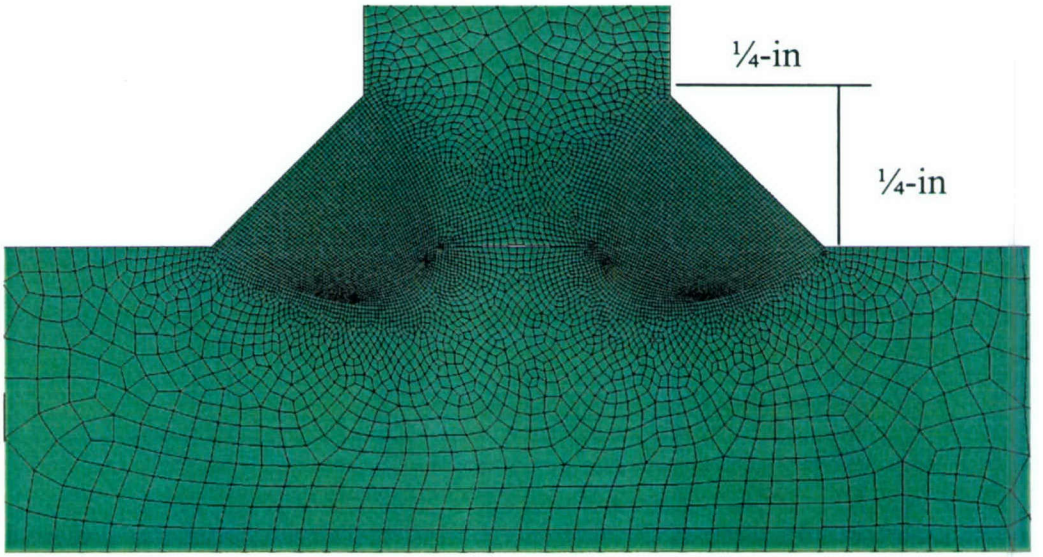

Figure 5 Finite element mesh near the weld region of the 2-dimensional cross-section model

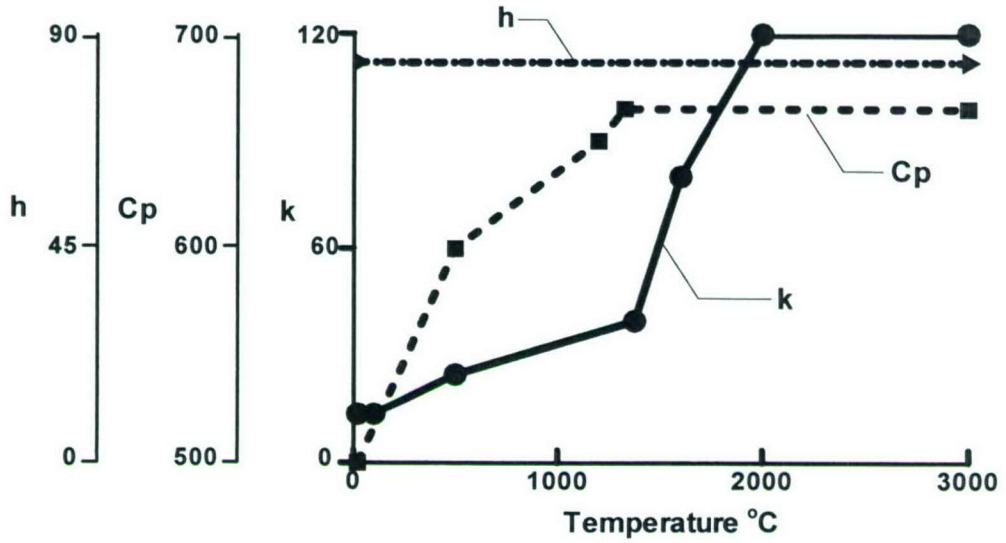

Figure 6 Temperature-dependent thermal conductivity, specific heat and convective heat loss coefficient used in this study (Ref. 16)

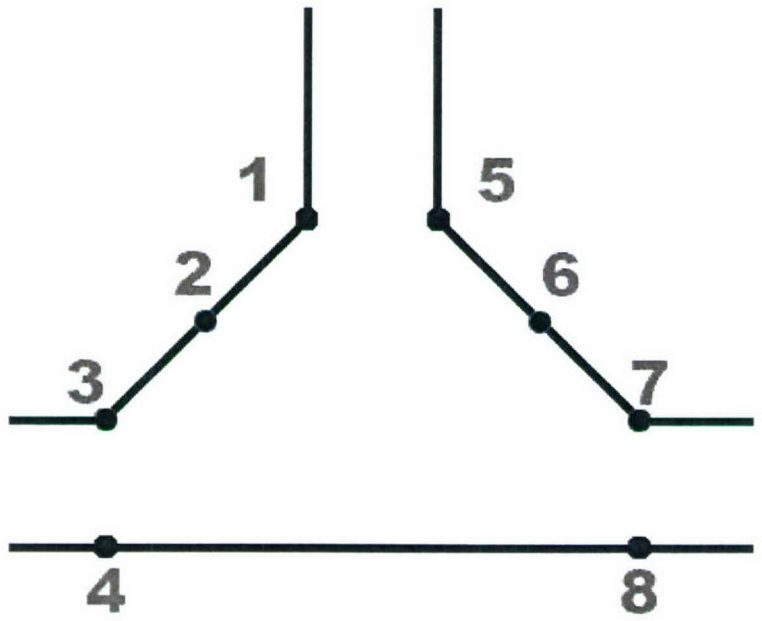

Figure 7 Selected eight locations around the two fillet welds for quantifying the sensitivity of material parameters on the temperature variation during welding

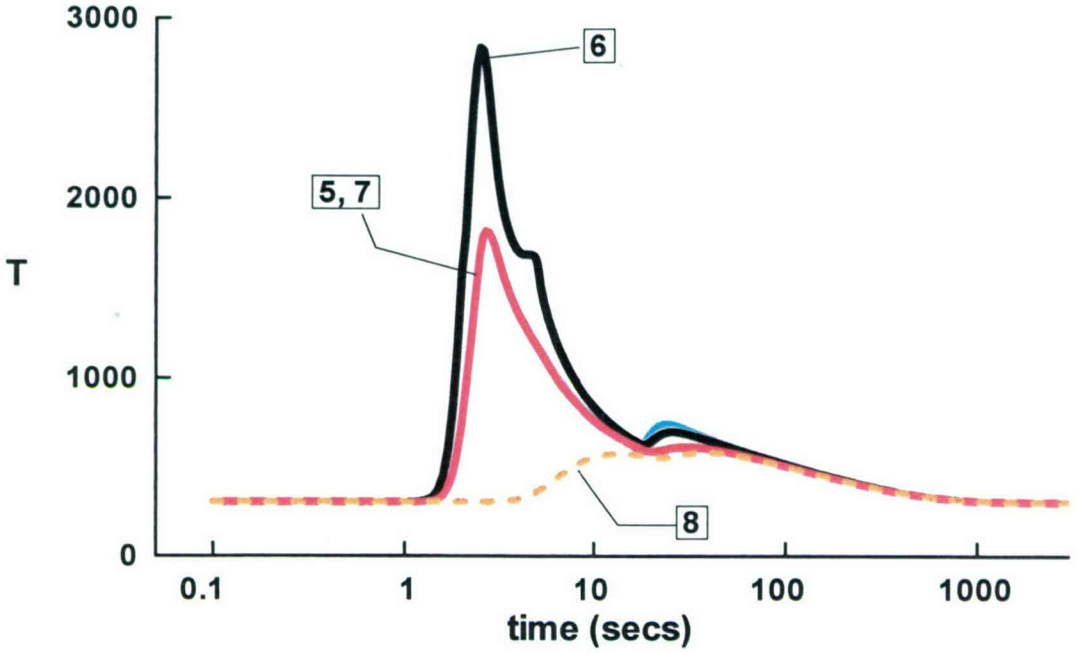

Figure 8 Variation of temperature as function of welding time at four different locations (Points 5 to 8) shown in Figure 7.

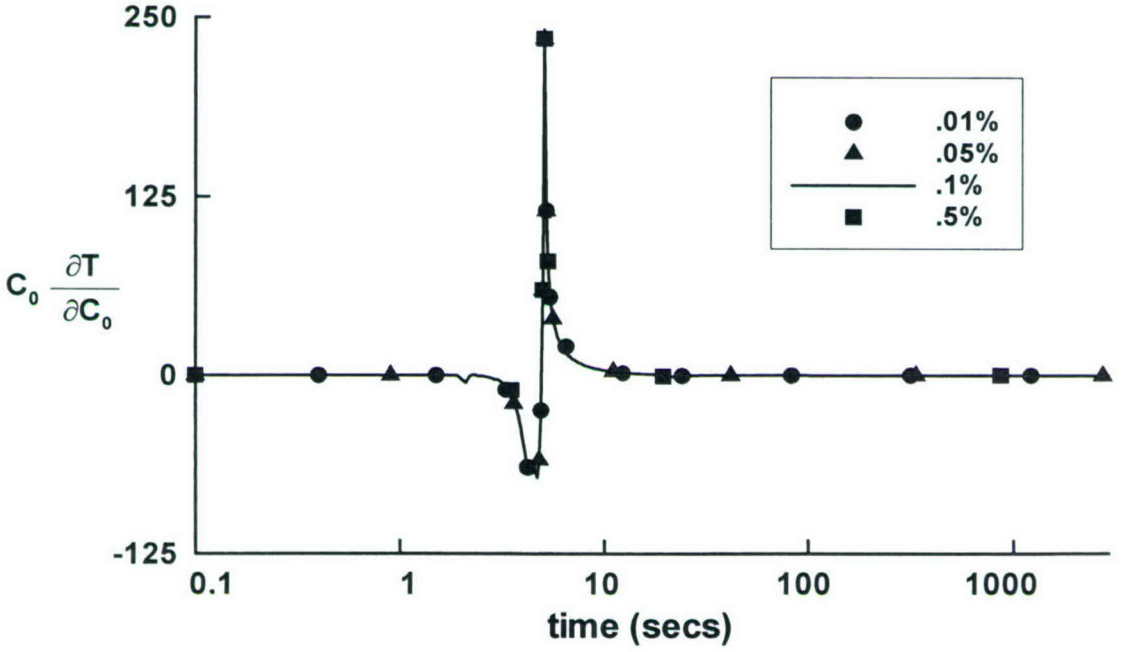

Figure 9 Time history of the "normalized" sensitivity of temperature with respect to the nominal alloy composition at the center of weld surface (Point 6 of Figure 7)

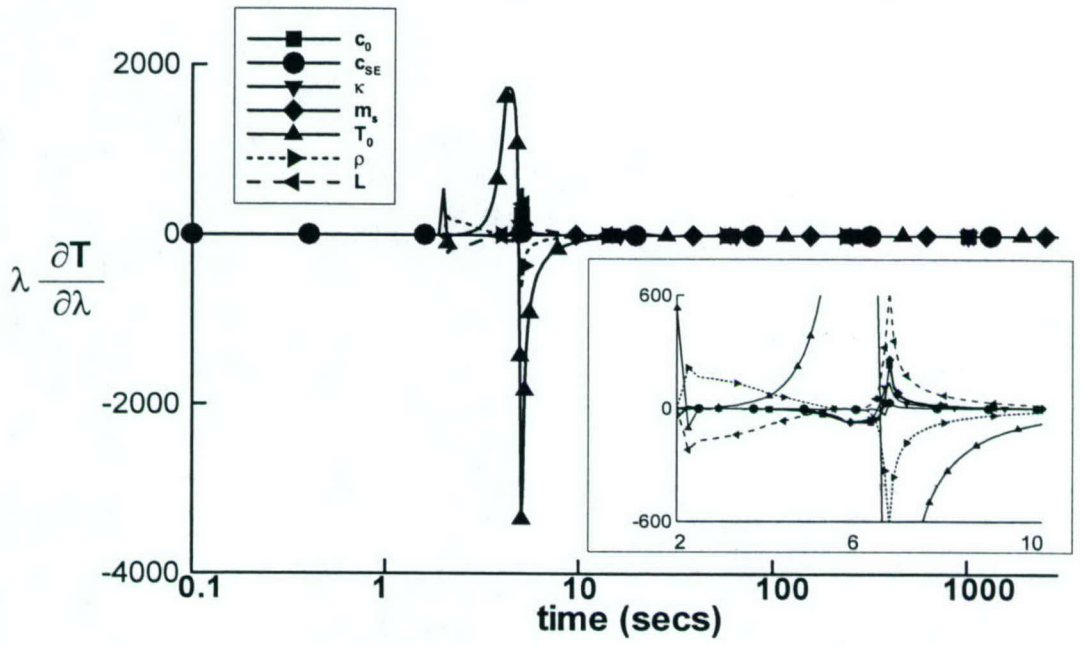

Figure 10 Time histories of the first-order sensitivity coefficient of the temperature with respect to the solidification parameters as the center point of weld surface (Point 6 of Figure 7).

Appendix I

List of Publications

1). Song, J., Peters, J., Noor, A., and Michaleris, P., Sensitivity Analysis of the Thermomechanical Response of Welded Joints. International Journal of Solids and Structures, (special issue honoring 70th Birthday of Arthur W. Leissa), Vol 40, No 16, August 2003, pp. 4167-4180.

2) Abdel-Tawab, Khaled and Noor, Ahmed K., Uncertainty Analysis of Welding Residual Stress Fields. Computer Methods in Applied Mechanics and Engineering, Vol. 179, Nos. 3-4, 1999, pp. 327-344.

3) Abdel-Tawab, Khaled and Noor, Ahmed K., A Fuzzy-Set Analysis for a Dynamic Thermo-elasto-viscoplastic Damage Response. Computers and Structures, Vol. 70, No. 1, Jan. 1999, pp. 91-107.

4) Noor, Ahmed K., Needleman, Alan and Peters, Jeanne M., Sensitivity Analysis for Failure and Damage in Dynamically Loaded Tensile Bars. Computer Methods in Applied Mechanics and Engineering, Vol. 151, Nos. 3-4, Jan. 1998, pp. 461-478.

Appendix II

Abstracts of Publications

1.) Sensitivity Analysis of the Thermomechanical Response of Welded Joints

A computational procedure is presented for evaluating the sensitivity coeffcients of the thermomechanical response of welded structures. Uncoupled thermo-mechanical analysis, with transient thermal analysis and quasi-static mechanical analysis, is performed. A rate independent, small deformation thermo-elasto-plastic material model with temperature dependent material properties is adopted in the study. The temperature field is assumed to be independent of the stresses and strains. The heat transfer equations emanating from a finite-element semi-discretization are integrated using an implicit backward-difference scheme to generate the time history of the temperatures. The mechanical response during welding is then calculated by solving a generalized plane strain problem. First- and second-order sensitivity coeffcients of the thermal and mechanical response quantities (derivatives with respect to various thermo-mechanical parameters) are evaluated using a direct differentiation approach in conjunction with an automatic differentiation software facility. Numerical results are presented for a double fillet conventional welding of a stiffener and a base plate made of stainless steel AL-6XN material. Time histories of the response and sensitivity coeffcients, and their spatial distributions at selected times are presented.

2.) Uncertainty Analysis of Welding Residual Stress Fields

A fuzzy-set approach is applied in conjunction with a finite element procedure to study the effect of uncertainty in material properties on welding residual stress fields. The study focuses on steels that undergo Martensitic transformations during the cool-down part of the weld thermal cycle. Uncoupled thermo-mechanical analysis is performed. Filler metal deposition, various convective-radiative energy losses, and latent heat generation are included in modeling of the welding process. A rate-independent thermo-elasto-plastic material model with nonlinear kinematic hardening is adopted in the study. Account is taken of the metallurgical transformations that occur during the entire weld thermal cycle. The material model is validated by comparing its predictions with existing experimental measurements of the welding residual mechanical fields. Fuzzy logic is then used to study the variability in the residual stress field due to pre-selected ranges of variation in material parameters associated with the Martensitic transformations. It is found that the variations in material parameters considered have a significant effect on the welding residual stress field.

3.) A Fuzzy-Set Analysis for a Dynamic Thermo-elasto-viscoplastic Damage Response

A computational fuzzy-set based approach is used to study variability (uncertainty) in the mechanical response of dynamically-loaded simple structural components. The mechanical response is described by a thermo-elasto-viscoplastic material model that accounts for damage. The uncertainty in the response is associated with pre-selected variations in material parameters. Sensitivity studies are performed to identify the material parameters which have the most significant effect on the response. Those parameters are then assumed to be fuzzy, and time histories of the possibility distributions of the response quantities are constructed. Numerical results are presented for a titanium alloy Ti-6A1-4V.

4.) Sensitivity Analysis for Failure and Damage in Dynamically Loaded Tensile Bars.

A computational procedure is presented for evaluating the sensitivity coefficients of porous viscoplastic solids under dynamic loading conditions. The effects of finite strains, material strain and strain-rate hardening, and the thermal softening due to adiabatic heating are incorporated into the formulation. A critical void volume fraction criterion is used to identify the initiation of failure. The equations of motion emanating from a finite element semi-discretization are integrated using an explicit central difference scheme. First- and second-order sensitivity coefficients of the response quantities (derivatives with respect to various material parameters) are evaluated using a direct differentiation approach in conjunction with an automatic differentiation software facility. Numerical results are presented for tensile specimens subjected to impact loading. Both axisymmetric and plane strain states are considered. The first- and second-order sensitivity coefficients are generated by evaluating the derivatives of the response quantities with respect to various macroscopic and microscopic material parameters. Time histories of the response and sensitivity coefficients, and their spatial distributions at selected times are presented.

Appendix III

Screenshots of Presentation on Residual Stresses and Distortions in Large Welded Structures

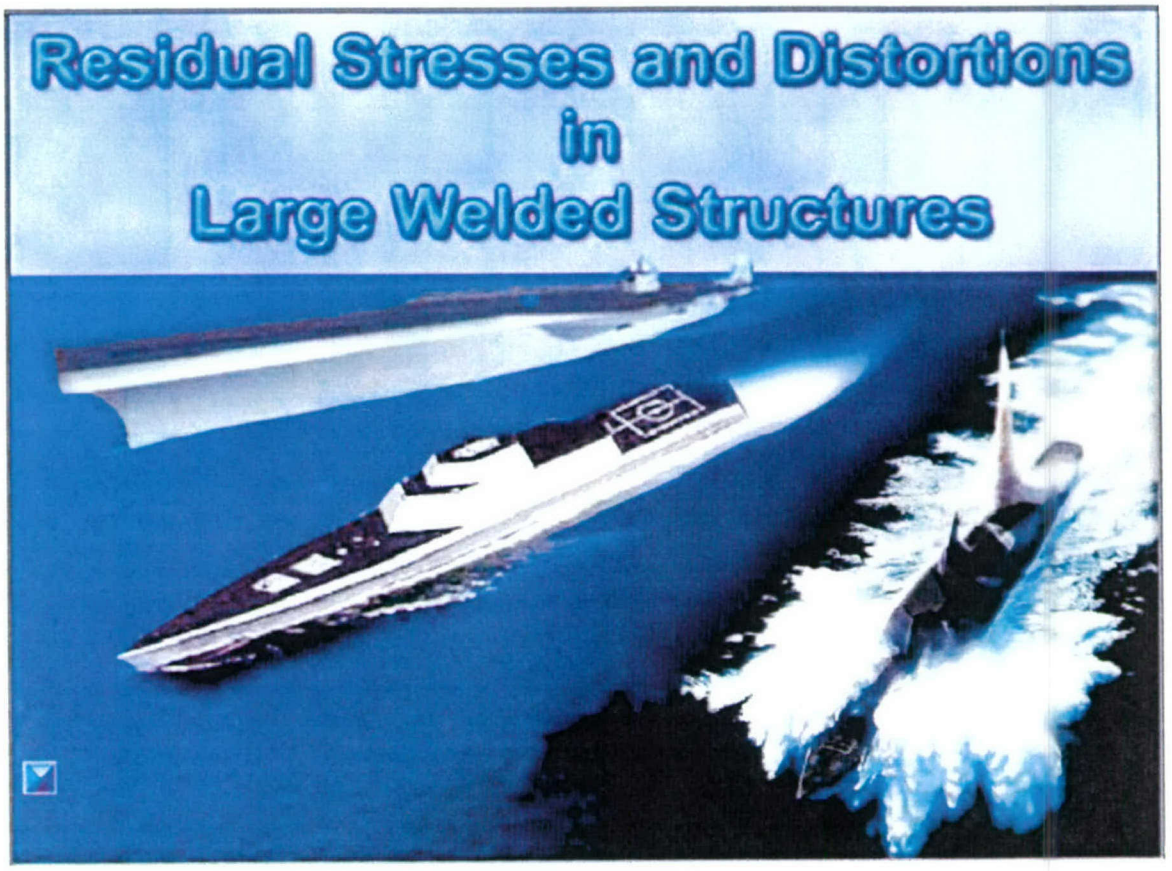

Future Work

- Assess the reliability of the materials models incorporating microscopic solidification and metallurgical transformation (with Oak Ridge, Lehigh University and Penn State teams)
  - Systematic verification, validation and calibration of models
- Explore processing methods for reducing residual stresses and distortions in stainless steel ADH fabrication (with Oak Ridge, Lehigh University, Penn State, and Navy Lab teams)
  - Effective use of sensitivity information

Main Menu

Future Work

- Apply the methodologies developed to large welded structures (with Oak Ridge, Navy Lab and other teams)

Main Menu


Sponsors
Office of
Naval Research
ONR
National Aeronautics and Space Administration
NASA

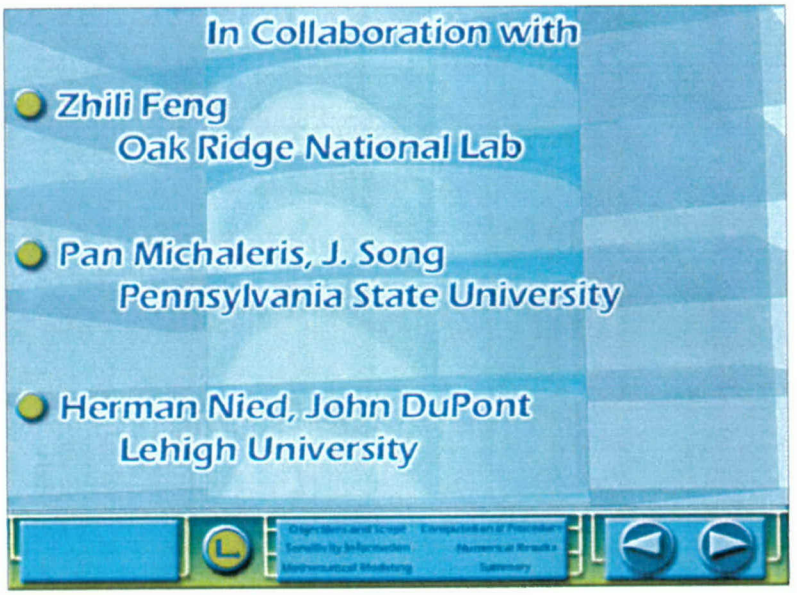
In Collaboration with
Zhili Feng
Oak Ridge National Lab
Pan Michaleris, J. Song
Pennsylvania State University
Herman Nied, John DuPont
Lehigh University

Outline

Objectives and Scope
Sensitivity Information
Mathematical Modeling
Computational Procedure
Numerical Results
Summary

Overall goals

- Develop models and establish effective methodologies for the reliable prediction of residual stresses, distortions and microstructure changes in welded components
- Study effect of residual stresses and microstructural changes on both brittle and ductile fracture behavior

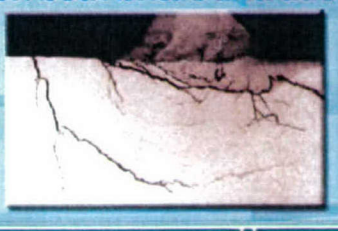

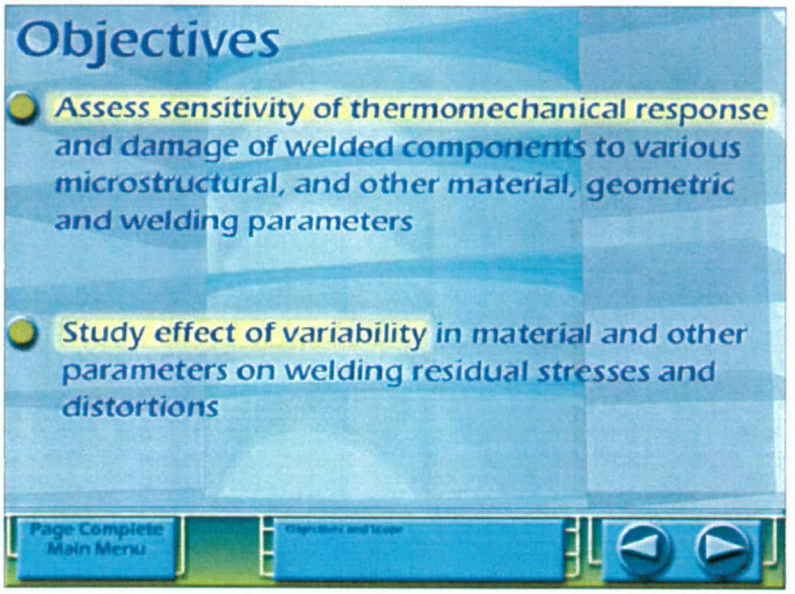
Objectives
Assess sensitivity of thermomechanical response and damage of welded components to various microstructural, and other material, geometric and welding parameters
Study effect of variability in material and other parameters on welding residual stresses and distortions
Page Complete
Main Menu

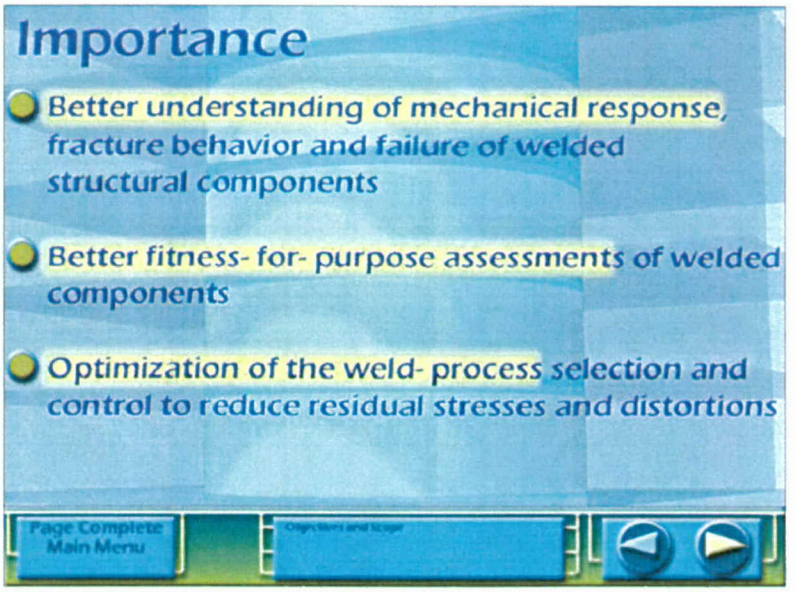
Importance
Better understanding of mechanical response, fracture behavior and failure of welded structural components
Better fitness- for- purpose assessments of welded components
Optimization of the weld- process selection and control to reduce residual stresses and distortions
Page Complete
Main Menu

Scope

- Stainless steel : AL-6XN
- Heat source model
- Heat transfer model incorporating microstructure solidification (Z. Feng)
- Rate independent thermo-elasto-plastic constitutive model

Page Complete
Main Menu

Uses

- Assess effect of uncertainties
- Predict changes in response
- Help in identifying regions of the structure requiring models with different length scales
- Identify changes in parameters required to achieve certain performance characteristics
- Determine search direction in optimization techniques

- Material and geometric parameters
- Weld characteristics

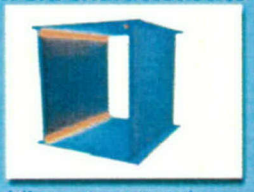

- Microstructural parameters

Page Complete
Main Menu

Approaches for Sensitivity Analysis

- Direct Differentiation
  - Automatic Differentiation (e.g., ADIFOR)
  - Jump discontinvities can occur. Regularization poses a challenge
- Finite Differences
  - F.D. increment must be chosen to avoid both truncation and round-off errors
- Mixed Hybrid Approaches

Main Menu

Governing Equations

Nonlinear Response:

$$\{ F(X, \lambda, t) \} = 0$$

$\{X\}$ = fundamental unknowns (response vector)

λ = typical system parameter

t = time

Sensitivity Coefficients:

$$\left\{\frac{\partial F}{\partial \lambda}\right\} + \left[\frac{\partial F}{\partial \lambda}\right]\left\{\frac{\partial X}{\partial \lambda}\right\} = 0$$

$\left\{\frac{\partial X}{\partial \lambda}\right\}$ = vector of sensitivity coefficients

Governing Equations

$\left\{\frac{\partial \hat{X}}{\partial \lambda}\right\}$ = vector of normalized sensitivity coefficients

= vector of norma

$$= \frac{\lambda_{ref}}{|X|_{ref}} \left\{\frac{\partial X}{\partial \lambda}\right\}$$

$$\frac{\{\Delta X\}}{|X|_{ref}} \cong \frac{\Delta \lambda}{\lambda_{ref}} \left\{\frac{\partial \hat{X}}{\partial \lambda}\right\}$$

Thermal, Mechanical and Metallurgical Couplings

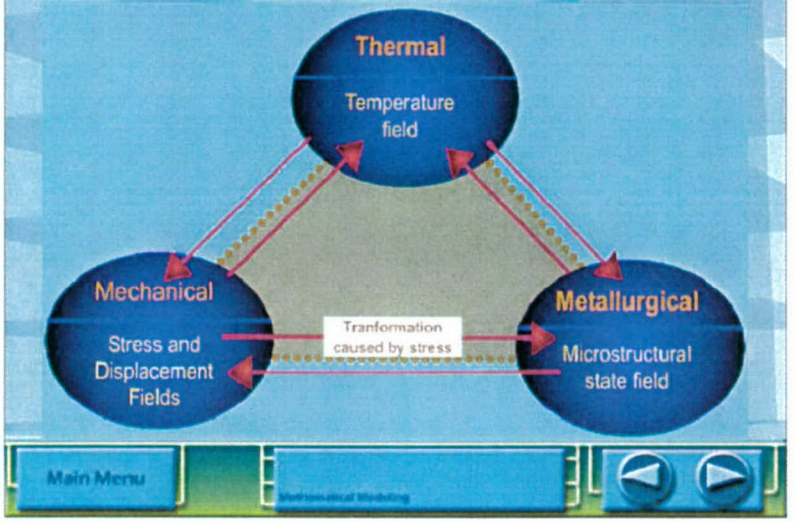

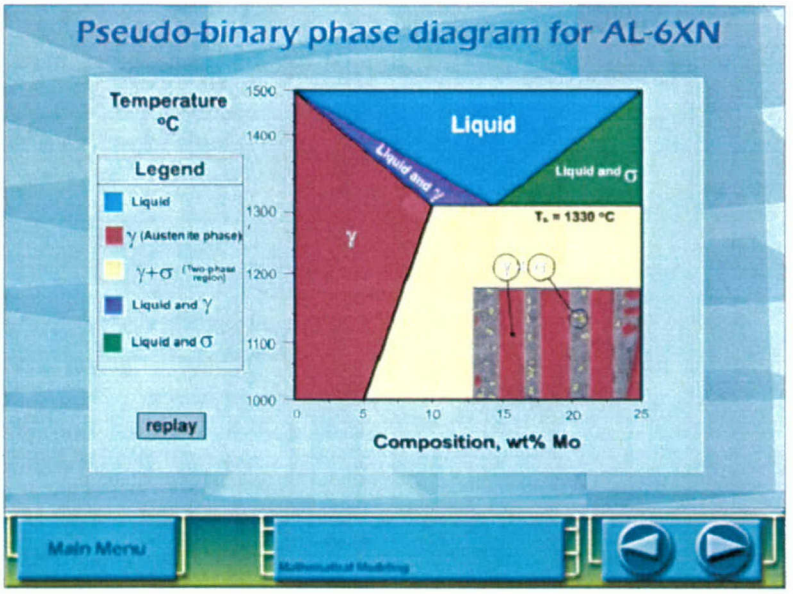
Pseudo-binary phase diagram for AL-6XN
Temperature °C
Legend
Liquid
γ (Austenite phase)
γ+σ (Two-phase region)
Liquid and γ
Liquid and σ
replay
Liquid
Liquid and γ
Liquid and σ
γ
T = 1330 °C
1500
1400
1300
1200
1100
1000
0
5
10
15
20
25
Composition, wt% Mo
Main Menu

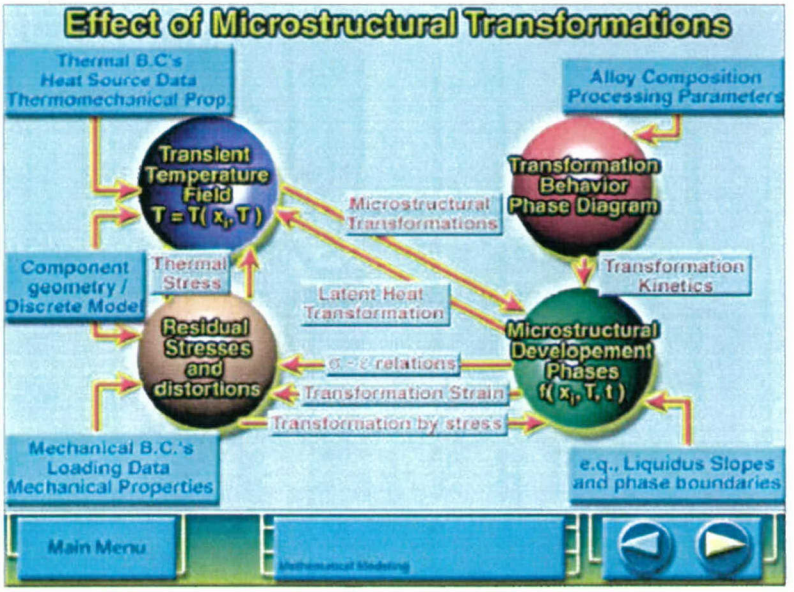
Effect of Microstructural Transformations
Thermal B.C's
Heat Source Data
Thermomechanical Prop
Alloy Composition
Processing Parameters
Transient Temperature Field
T = T(x_i, T)
Transformation Behavior Phase Diagram
Microstructural Transformations
Component geometry / Discrete Model
Thermal Stress
Transformation Kinetics
Latent Heat Transformation
Residual Stresses and distortions
Microstructural Developement Phases
f(x_i, T, t)
σ - ε relations
Transformation Strain
Transformation by stress
Mechanical B.C.'s
Loading Data
Mechanical Properties
e.g., Liquidus Slopes and phase boundaries
Main Menu

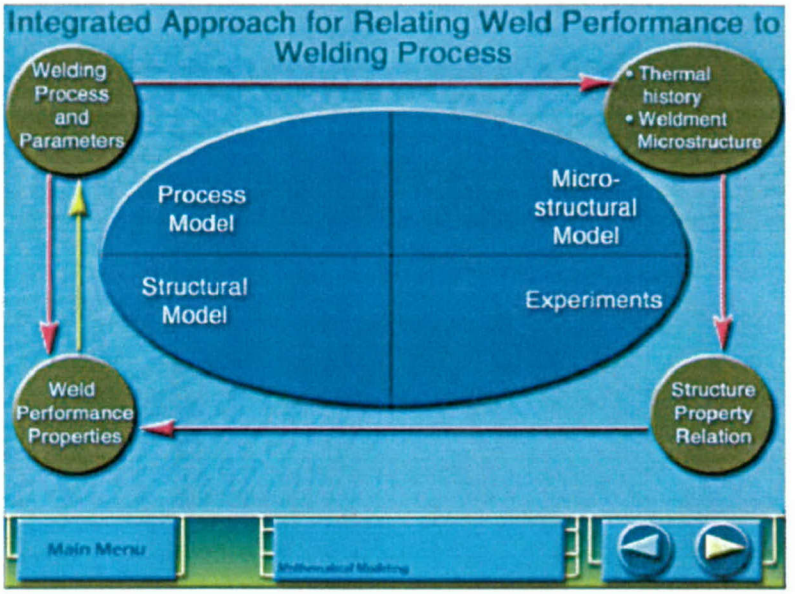
Integrated Approach for Relating Weld Performance to Welding Process
Welding Process and Parameters
• Thermal history
• Weldment Microstructure
Process Model
Micro-structural Model
Structural Model
Experiments
Weld Performance Properties
Structure Property Relation
Main Menu

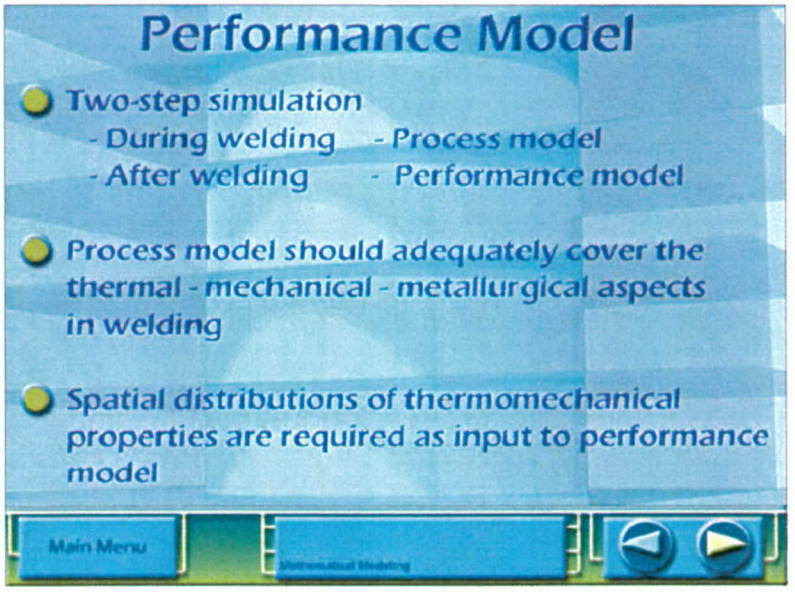
Performance Model
Two-step simulation
- During welding - Process model
- After welding - Performance model
Process model should adequately cover the thermal - mechanical - metallurgical aspects in welding
Spatial distributions of thermomechanical properties are required as input to performance model
Main Menu

Welding Heat Input
Double Ellipsoid Model (Goldak et al.)

$$q = \frac{6\sqrt{3}\, f\, (\eta\, U\, I)}{a\, b\, c\, \pi\sqrt{\pi}}\; e^{-\left[\frac{3y^2}{b^2} + \frac{3z^2}{c^2} + \frac{3(x+vt)^2}{a^2}\right]}$$

q = power density in front (and rear) ellipsoids

a = b, f = 0.6 before the torch passes the analysis plane

a = 4b, f = 1.4 after the torch passes the analysis plane

b, c weld width penetration

f = fractions of heat deposited

η, U, I = welding efficiency, voltage and amperage

x, y, z = local coordinates of double ellipsoid model

v = torch travel speed

Heat Transfer Model
(Incorporating Microstructure Solidification)

- AL6XN (and other stainless steels) solidifies under unequilibrium conditions due to the rapid cooling in the weld pool
- Under the welding conditions characteristic to this study, the unequilibrium solidification process results in formation of dendrite microstructure in the weld pool (constitutional super-cooling) [DuPont, private communications]
- The grain morphology is simplified as cellular cells

Main Menu

Heat Transfer Model
(Incorporating Microstructure Solidification - Feng)

$$\nabla \bullet (\kappa \nabla T) + Q = \rho C_p \dot{T}$$

κ = temperature-dependent conductivity

The release of latent heat from formation of dendrite microstructure is treated as an internal heat generation term in the heat flow, Q

ρ = mass density

C_p = temperature-dependent specific heat

Heat Transfer Model
(Incorporating Microstructure Solidification - Feng)

$$Q = \begin{cases} q_i & for\ T_s < T < T_L \\ 0 & for\ T < T_s,\ or\ T > T_L \end{cases}$$

The release of latent heat during weld solidification is determined from the rate of dendrite formation

q_i = Rate of latent heat release

T_s = Solidus temperature

T_L = Liquidus temperature

Heat Transfer Model
(Incorporating Microstructure Solidification - Feng)

$$q_l = L\frac{\partial f_s}{\partial t}$$

L = total energy released during solidification per unit volume (volumetric latent heat)

f_s = fraction of solid during welding related to the composition at the solid-liquid interface C_s by the local solute redistribution equation

The solidification rate is linked to the cooling rate through Fleming's local solute distribution equation, and phase diagrams

Heat Transfer Model
(Incorporating Microstructure Solidification - Feng)

$$q_l = L\frac{\partial f_s}{\partial C_s^*}\frac{\partial C_s^*}{\partial T}\frac{\partial T}{\partial t}$$

$$= \frac{L(kC_o)^{\frac{1}{1-k}}}{m_s(1-k)}\left[\frac{T-T_s+C_{SE}}{m_s}\right]^{\frac{2-k}{k-1}}\frac{\partial T}{\partial t}$$

m_s = Solidus slope C_{SE} = Maximum solid solubility

C_o = nominal alloy composition

$\kappa = \dfrac{\text{liquidus slope } m_L}{\text{solidus slope } m_s}$

= equilibrium distribution coefficient (partition ratio)

T_s = Solidus temperature

Heat Transfer Model
(Incorporating Microstructure Solidification - Feng)

- Surface heat loss from convection and radiation are included as boundary conditions

$$q_{loss} = h(T - T_\infty) - \sigma\varepsilon\left(T^4 - T_\infty^4\right)$$

h = convection coefficient

$\sigma\varepsilon$ = radiation coefficient

Cross Section of Fillet Weld
Details of HAZ (AL-6XN)

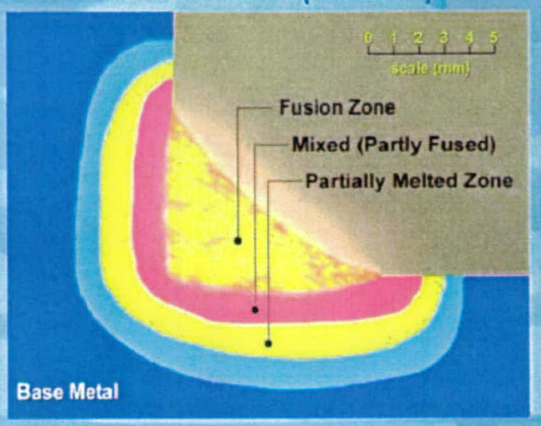

Main Menu

Modeling Metal Deposition

- First assign artificially soft properties to all the elements to be welded later
- Switch back to the actual properties on integration point basis once it begins to solidify from weld pool
- Switching is done based on temperature to avoid numerical convergence problems
- Unrealistic plastic strains in the weld pool due to solid mechanics formulation are also eliminated upon switching
- Element rebirth is done on pass, not elements

Main Menu

Computational Procedure

Finite Element Implementation

$$\dot{\varepsilon}^{\mathrm{tm}} = \dot{\varepsilon}^{\mathrm{th}} + \dot{\varepsilon}^{\mathrm{tr}} + \dot{\varepsilon}^{\mathrm{tp}} = \mathbf{A}(T, \xi_A, \xi_M, \xi_L, \sigma)\ \dot{T}$$

ε^{tm} = thermo-metallurgical strain tensor

Main Menu

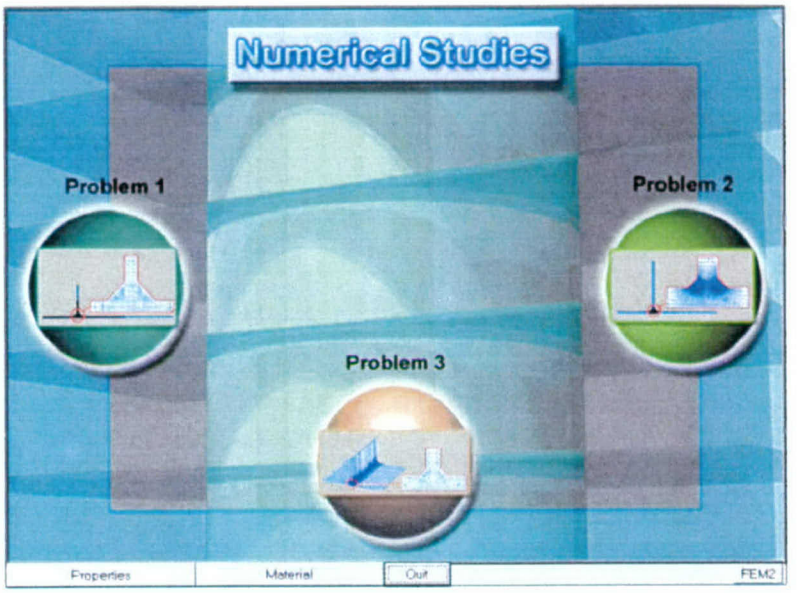
Numerical Studies
Problem 1
Problem 2
Problem 3
Properties
Material
Out
FEM2


Double Fillet Conventional Welding
of a stiffener and a base plate
Menu
Replay

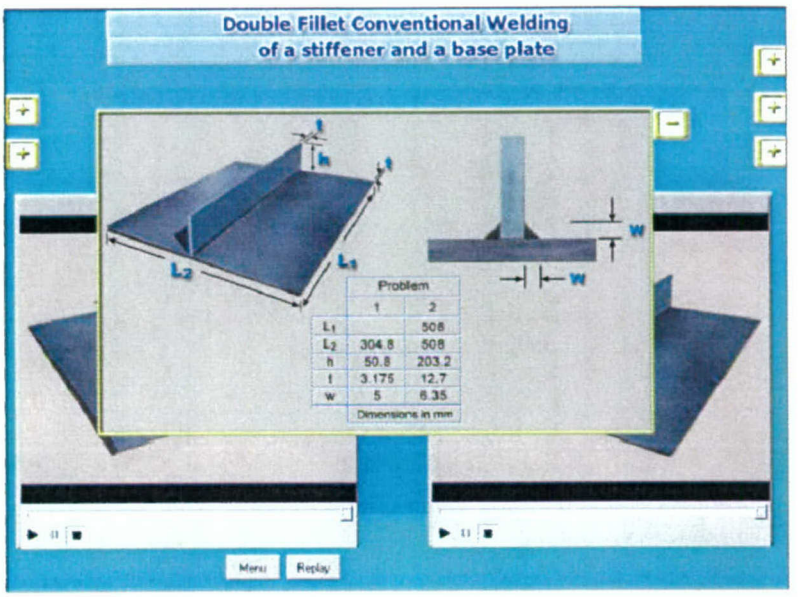
Double Fillet Conventional Welding
of a stiffener and a base plate
t
h
t
L2
L1
w
w
Problem
1
2
L1
508
L2
304.8
508
h
50.8
203.2
t
3.175
12.7
w
5
6.35
Dimensions in mm
Menu
Replay

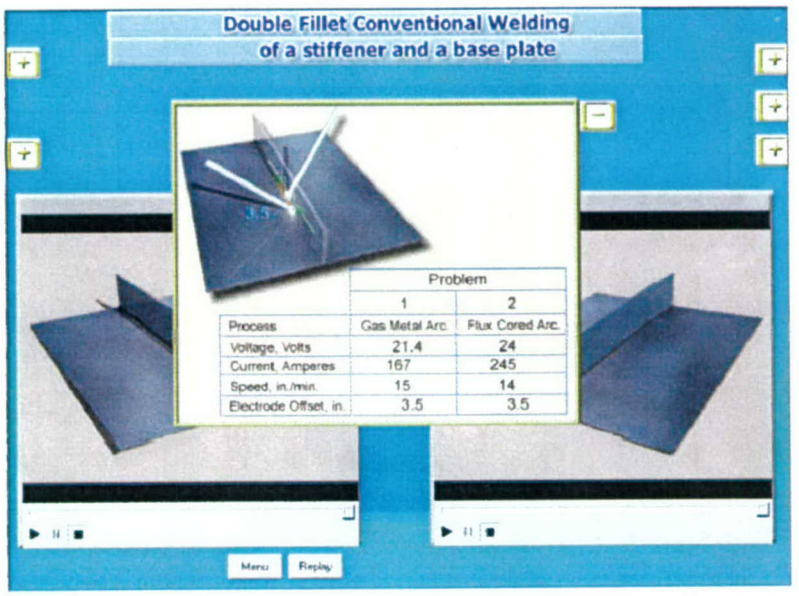
Double Fillet Conventional Welding
of a stiffener and a base plate
Problem
1
2
Process
Gas Metal Arc
Flux Cored Arc
Voltage, Volts
21.4
24
Current, Amperes
167
245
Speed, in./min.
15
14
Electrode Offset, in.
3.5
3.5
Menu
Replay

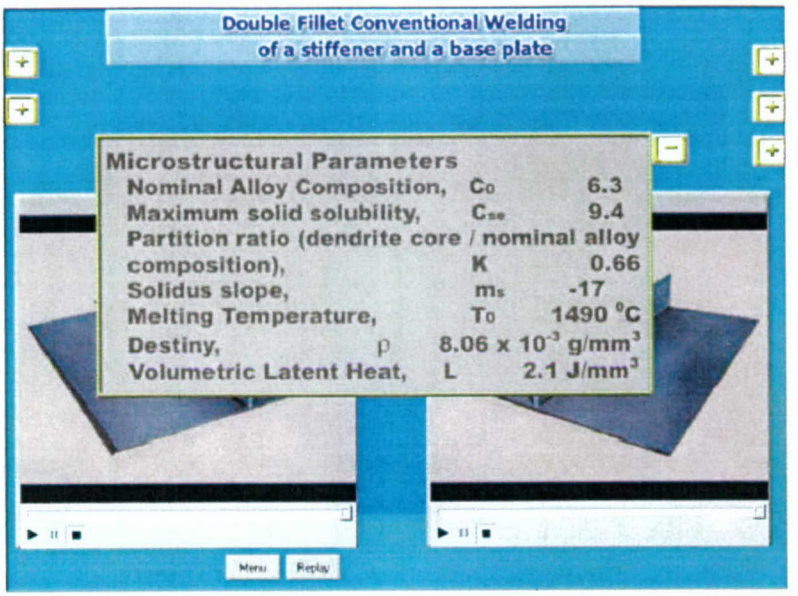
Double Fillet Conventional Welding
of a stiffener and a base plate
Microstructural Parameters
Nominal Alloy Composition, C_0 6.3
Maximum solid solubility, C_{se} 9.4
Partition ratio (dendrite core / nominal alloy composition), K 0.66
Solidus slope, m_s -17
Melting Temperature, T_0 1490 °C
Destiny, ρ 8.06×10^{-3} g/mm³
Volumetric Latent Heat, L 2.1 J/mm³
Menu
Replay

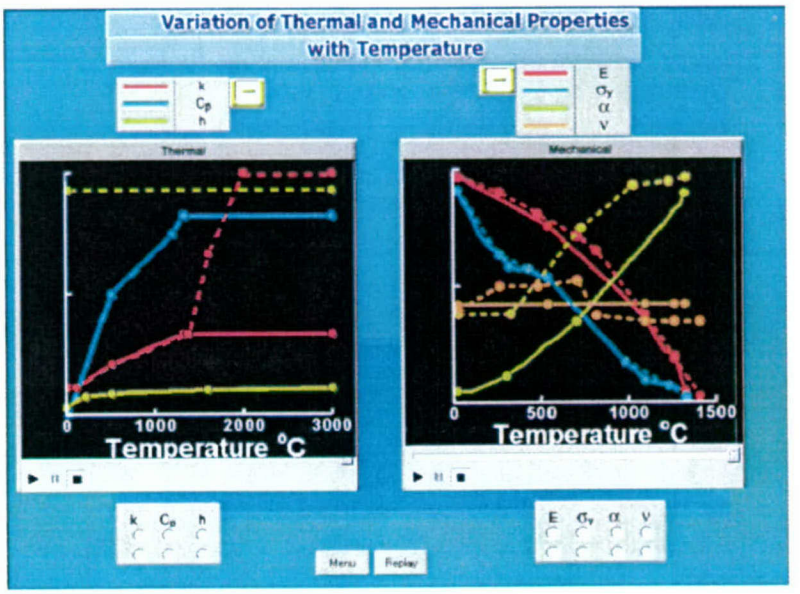
Variation of Thermal and Mechanical Properties
with Temperature
k
Cp
h
E
σy
α
ν
Thermal
0
1000
2000
3000
Temperature °C
Mechanical
0
500
1000
1500
Temperature °C
Menu
Replay

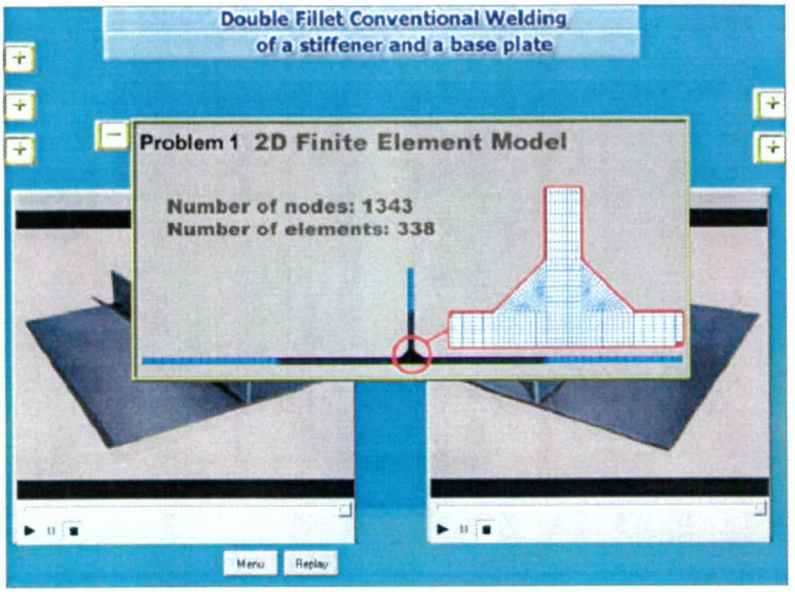
Double Fillet Conventional Welding
of a stiffener and a base plate
Problem 1 2D Finite Element Model
Number of nodes: 1343
Number of elements: 338
Menu
Replay

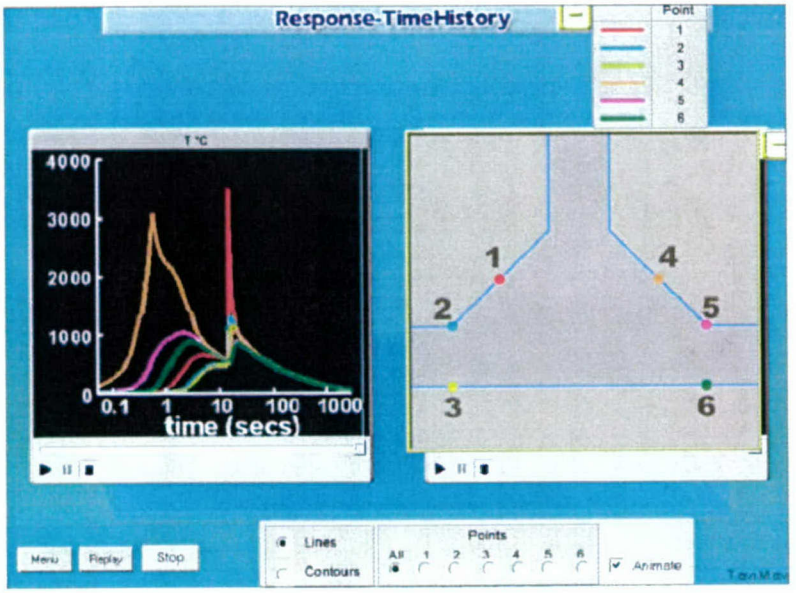
Response-TimeHistory
Point
1
2
3
4
5
6
T °C
4000
3000
2000
1000
0
0.1
1
10
100
1000
time (secs)
1
2
3
4
5
6
Menu
Replay
Stop
Lines
Contours
Points
All
Animate

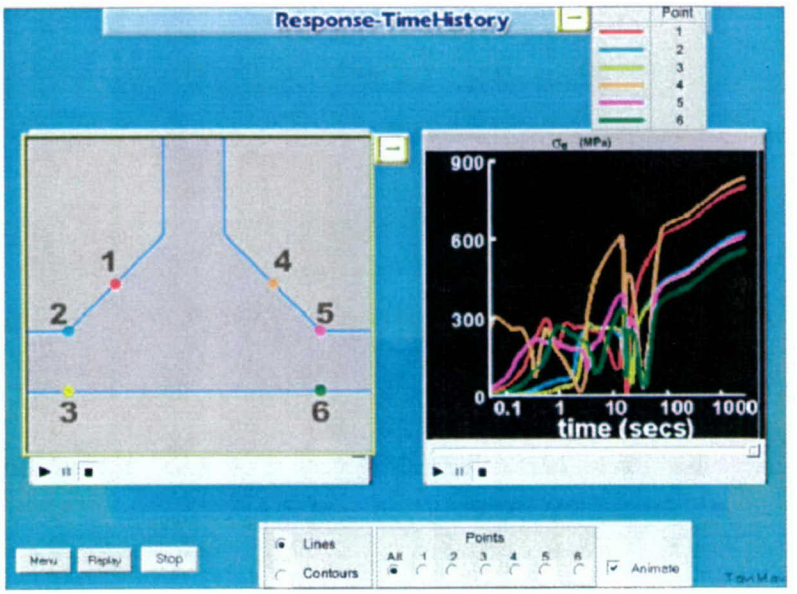
Response-TimeHistory
Point
1
2
3
4
5
6
1
2
3
4
5
6
900
600
300
0
0.1
1
10
100
1000
time (secs)
Menu
Replay
Stop
Lines
Contours
Points
All
Animate

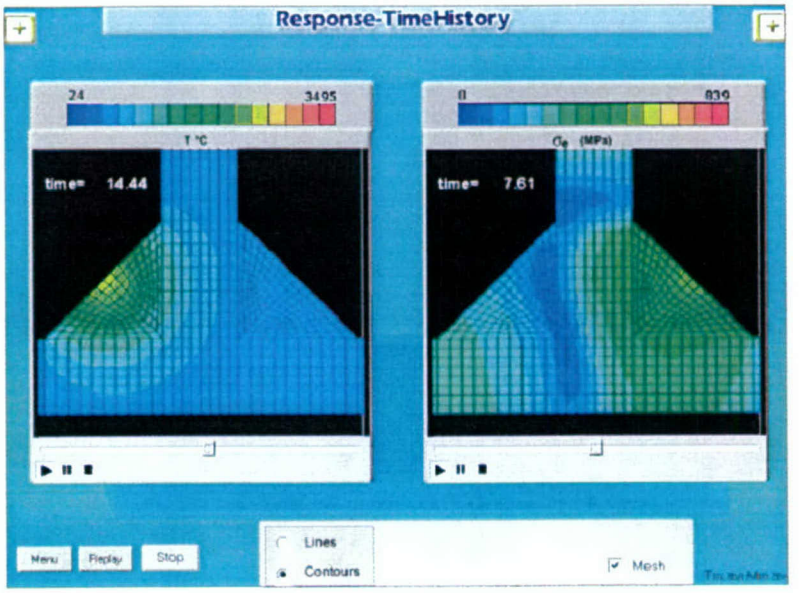
Response-TimeHistory
24
3495
T °C
time= 14.44
0
830
time= 7.61
Menu
Replay
Stop
Lines
Contours
Mesh

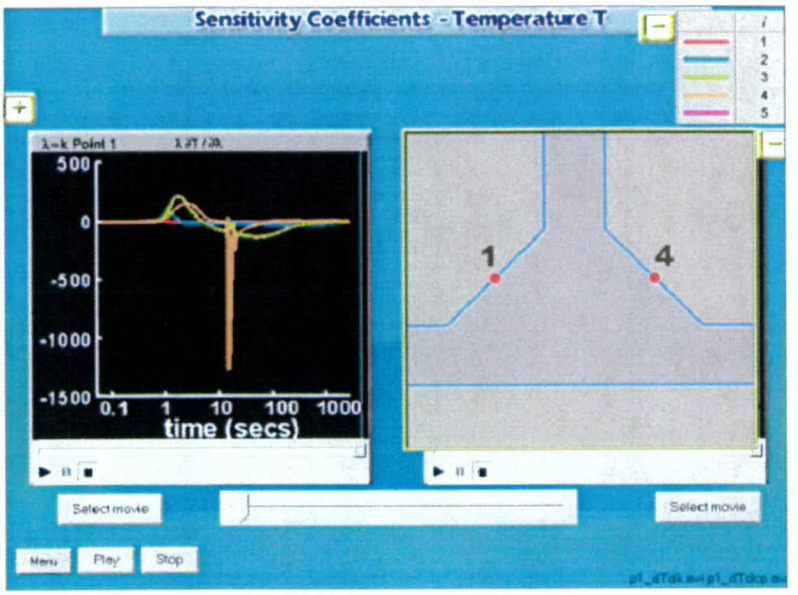
Sensitivity Coefficients - Temperature T
i
1
2
3
4
5
λ=k Point 1
λ∂T / ∂k
500
0
-500
-1000
-1500
0.1
1
10
100
1000
time (secs)
1
4
Select movie
Select movie
Menu
Play
Stop

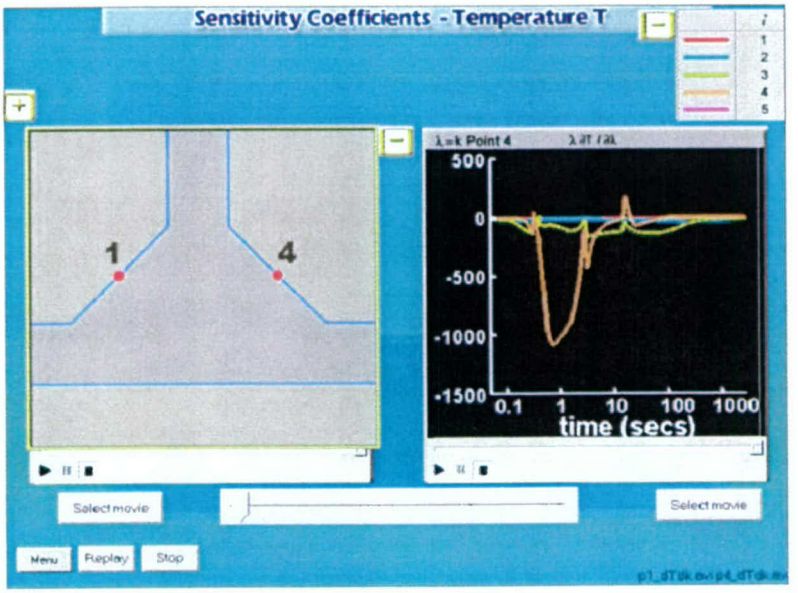
Sensitivity Coefficients - Temperature T
i
1
2
3
4
5
λ=k Point 4
λ∂T / ∂k
500
0
-500
-1000
-1500
0.1
1
10
100
1000
time (secs)
1
4
Select movie
Select movie
Menu
Replay
Stop

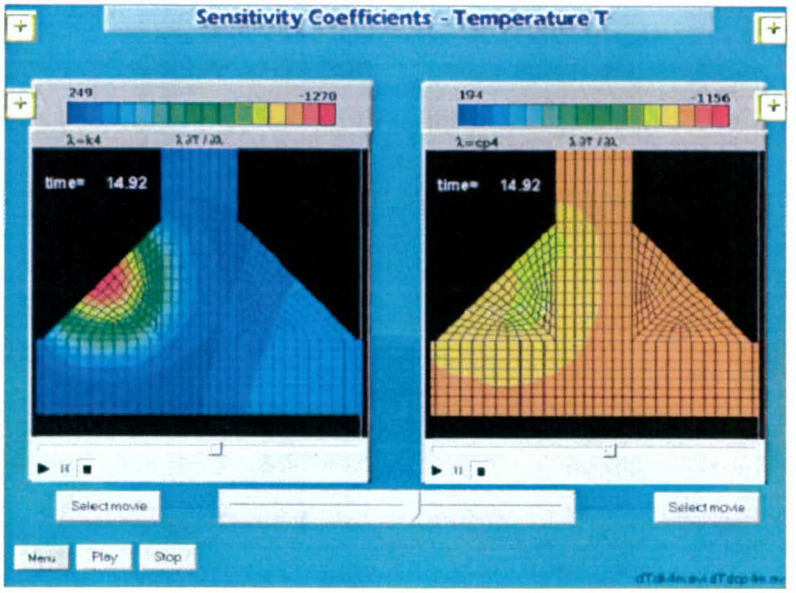
Sensitivity Coefficients - Temperature T
249
-1270
time= 14.92
194
-1156
time= 14.92
Select movie
Select movie
Menu
Play
Stop

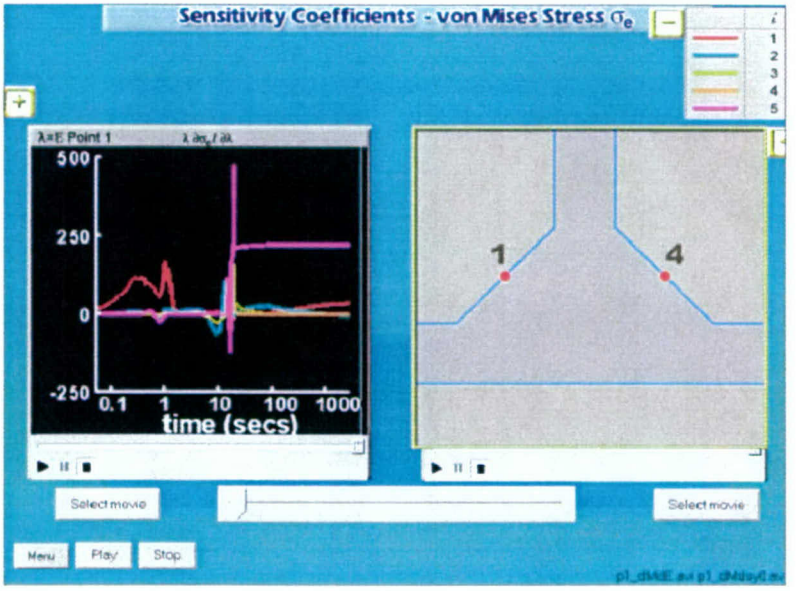
Sensitivity Coefficients - von Mises Stress σe
1
2
3
4
5
500
250
0
-250
0.1
1
10
100
1000
time (secs)
1
4
Select movie
Select movie
Menu
Play
Stop

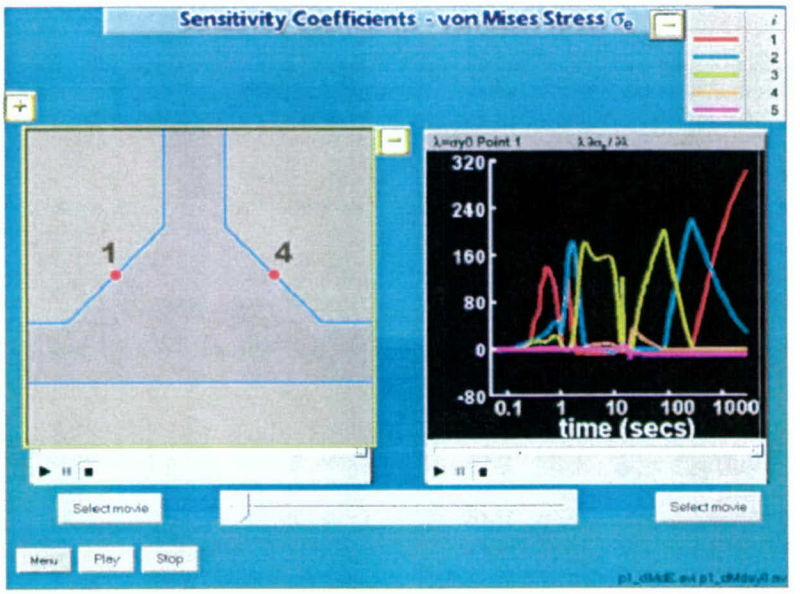
Sensitivity Coefficients - von Mises Stress σ_e
1
2
3
4
5
1
4
320
240
160
80
0
-80
0.1
1
10
100
1000
time (secs)
Select movie
Select movie
Menu
Play
Stop

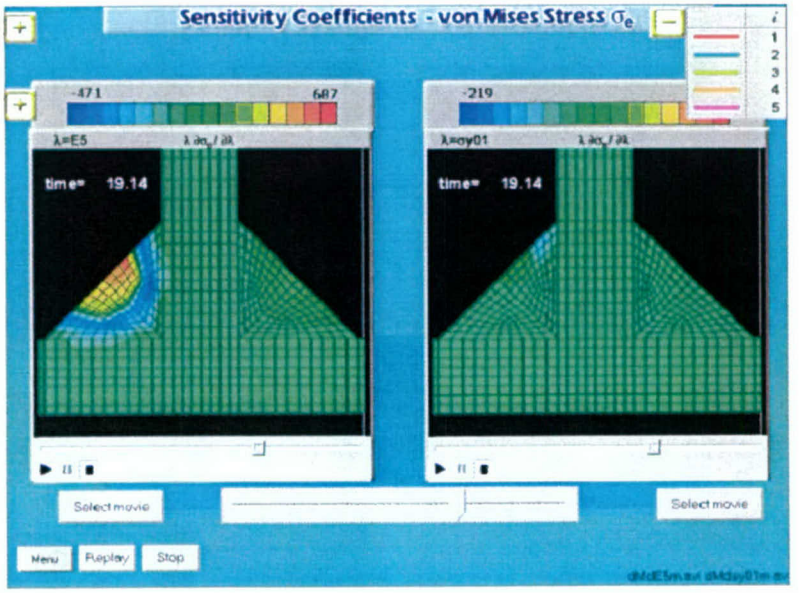
Sensitivity Coefficients - von Mises Stress σ_e
1
2
3
4
5
-471
687
-219
time= 19.14
time= 19.14
Select movie
Select movie
Menu
Replay
Stop

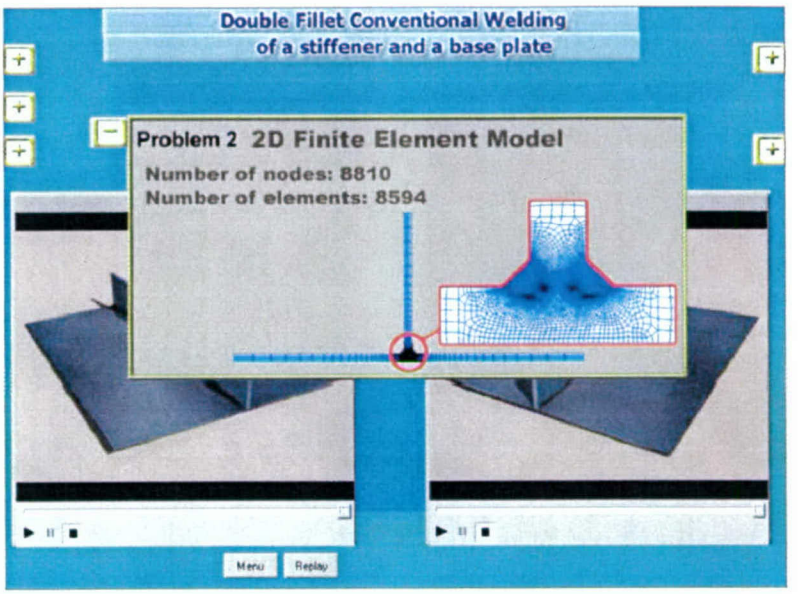
Double Fillet Conventional Welding
of a stiffener and a base plate
Problem 2 2D Finite Element Model
Number of nodes: 8810
Number of elements: 8594
Menu
Replay

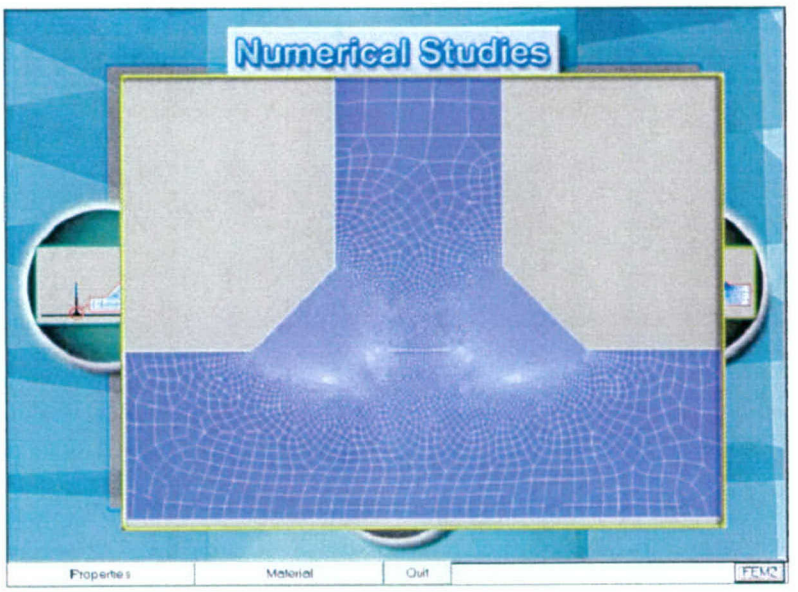
Numerical Studies
Properties
Material
Out
FEM2

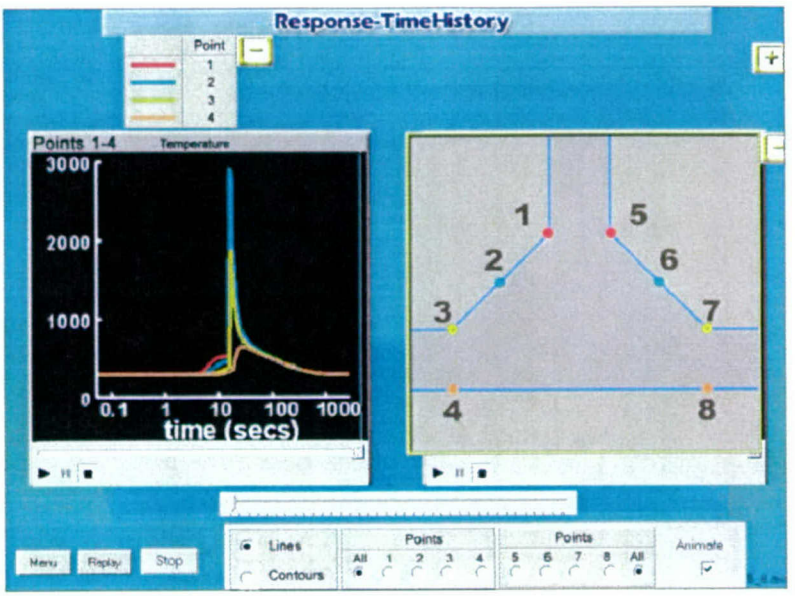
Response-TimeHistory
Point
1
2
3
4
Points 1-4
Temperature
3000
2000
1000
0
0.1
1
10
100
1000
time (secs)
1
2
3
4
5
6
7
8
Menu
Replay
Stop
Lines
Contours
Points
All
1
2
3
4
Points
5
6
7
8
All
Animate

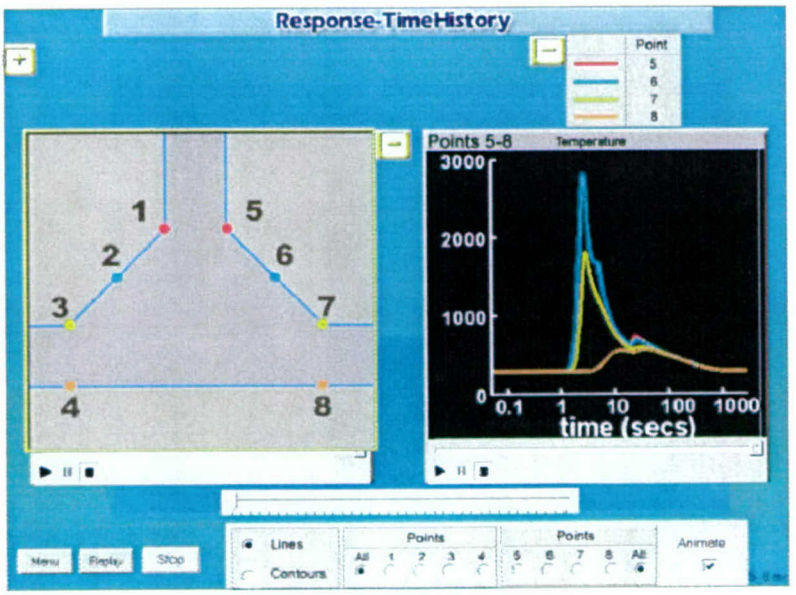
Response-TimeHistory
Point
5
6
7
8
Points 5-8
Temperature
3000
2000
1000
0
0.1
1
10
100
1000
time (secs)
1
2
3
4
5
6
7
8
Menu
Replay
Stop
Lines
Contours
Points
All
1
2
3
4
Points
5
6
7
8
All
Animate

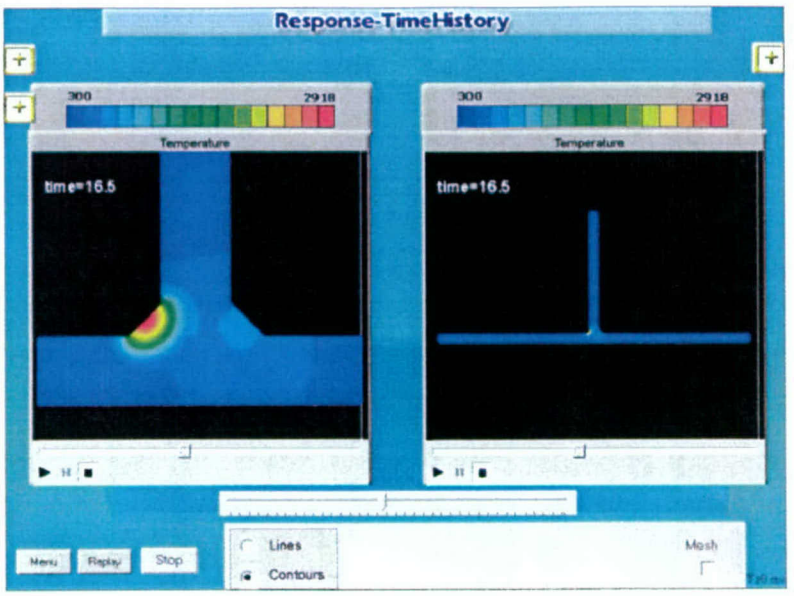
Response-TimeHistory
300
2918
Temperature
time=16.5
300
2918
Temperature
time=16.5
Menu
Replay
Stop
Lines
Contours
Mesh

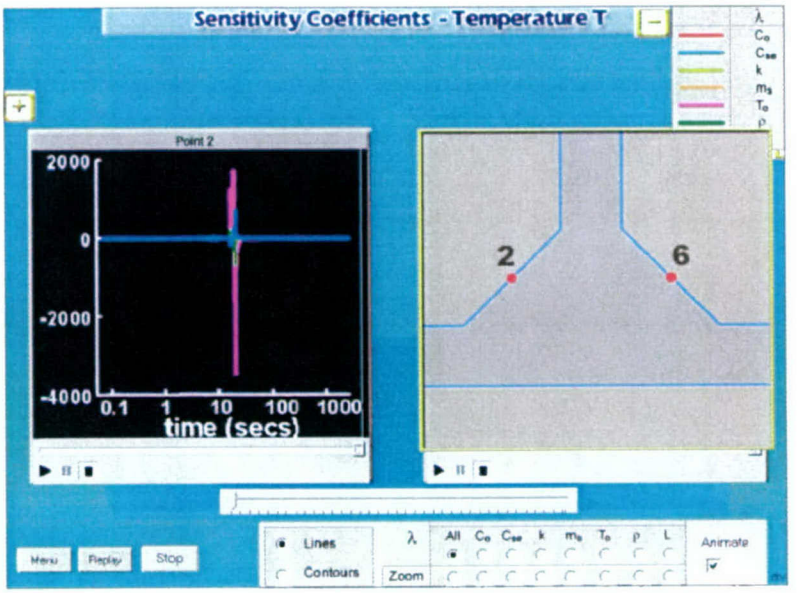
Sensitivity Coefficients - Temperature T
Point 2
2000
0
-2000
-4000
0.1
1
10
100
1000
time (secs)
2
6
Menu
Replay
Stop
Lines
Contours
Zoom
All
Animate

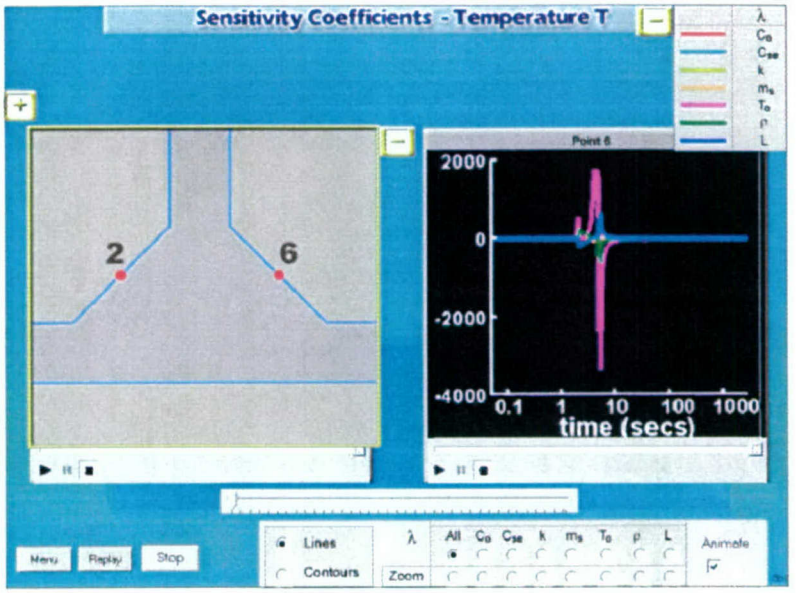
Sensitivity Coefficients - Temperature T
2
6
Point 6
2000
0
-2000
-4000
0.1
1
10
100
1000
time (secs)
Menu
Replay
Stop
Lines
Contours
Zoom
Animate

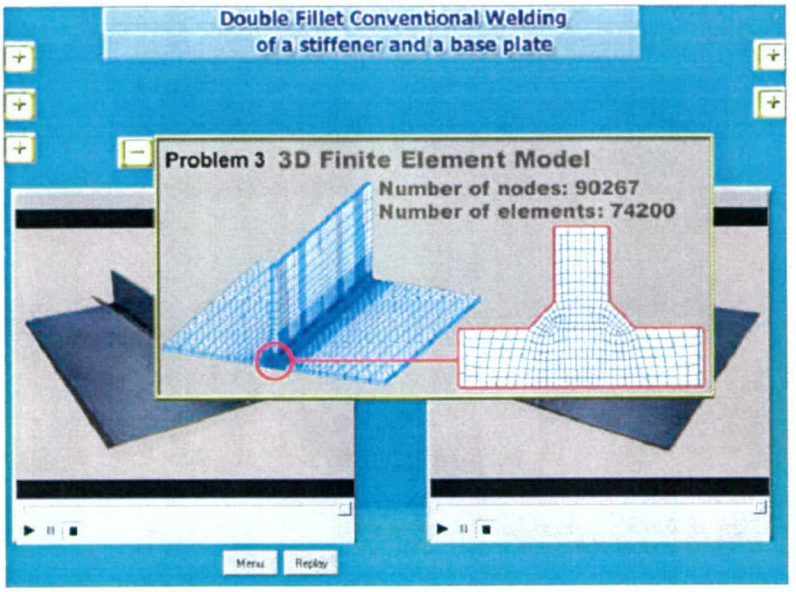
Double Fillet Conventional Welding
of a stiffener and a base plate
Problem 3 3D Finite Element Model
Number of nodes: 90267
Number of elements: 74200
Menu
Replay

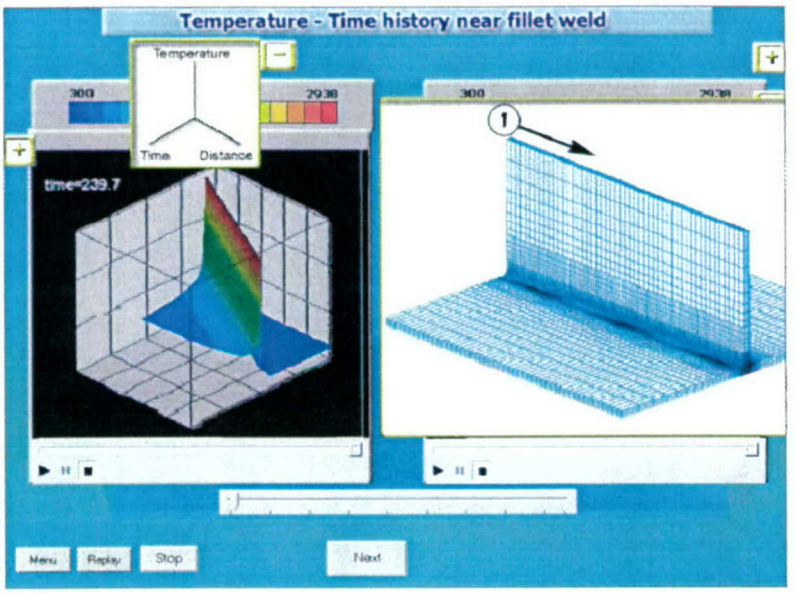
Temperature - Time history near fillet weld
Temperature
Time
Distance
300
2938
time=239.7
1
Menu
Replay
Stop
Next

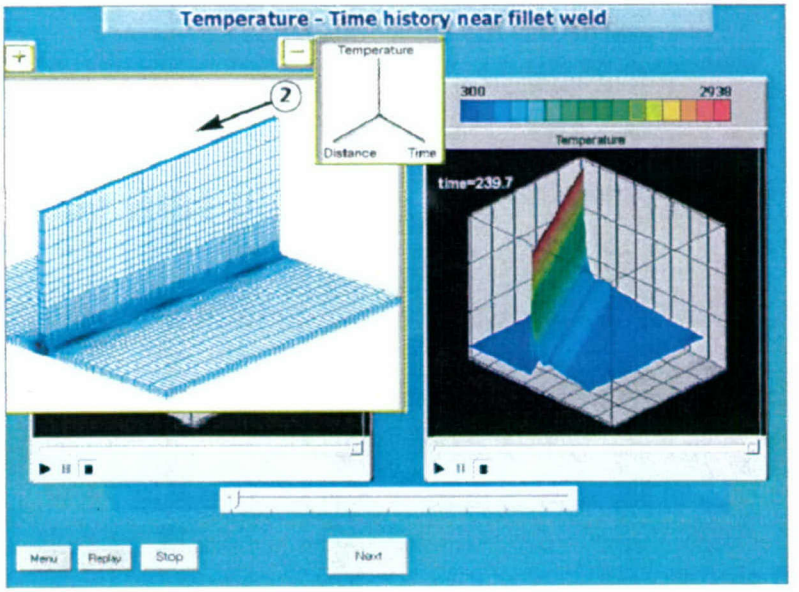
Temperature - Time history near fillet weld
Temperature
Distance
Time
2
300
2938
Temperature
time=239.7
Menu
Replay
Stop
Next

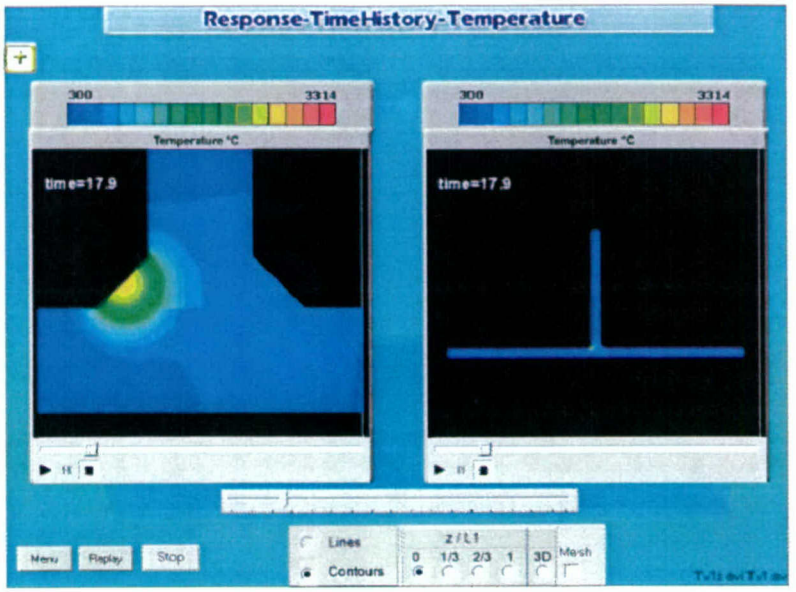
Response-TimeHistory-Temperature
300
3314
Temperature °C
time=17.9
300
3314
Temperature °C
time=17.9
Menu
Replay
Stop
Lines
Contours
z / L1
0
1/3
2/3
1
3D
Mesh

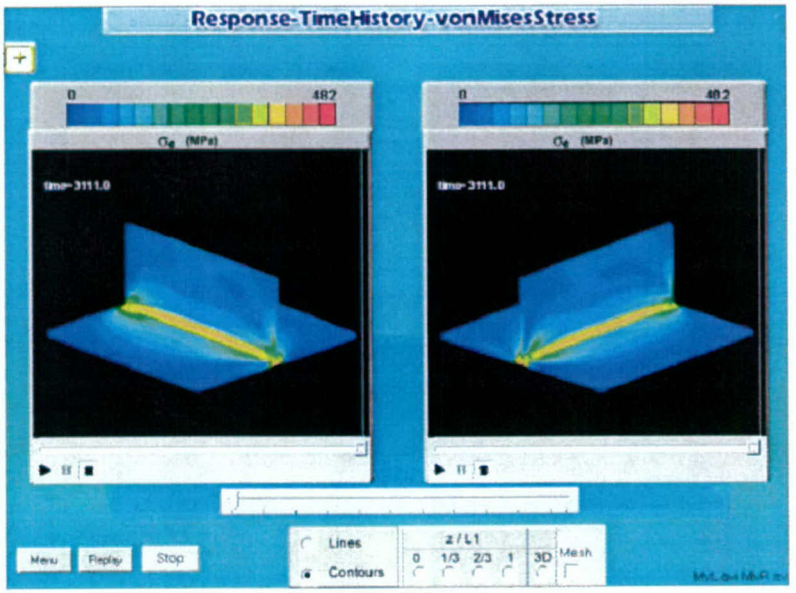
Response-TimeHistory-vonMisesStress
0
482
0
482
Menu
Replay
Stop
Lines
Contours
z / L1
0
1/3
2/3
1
3D
Mesh

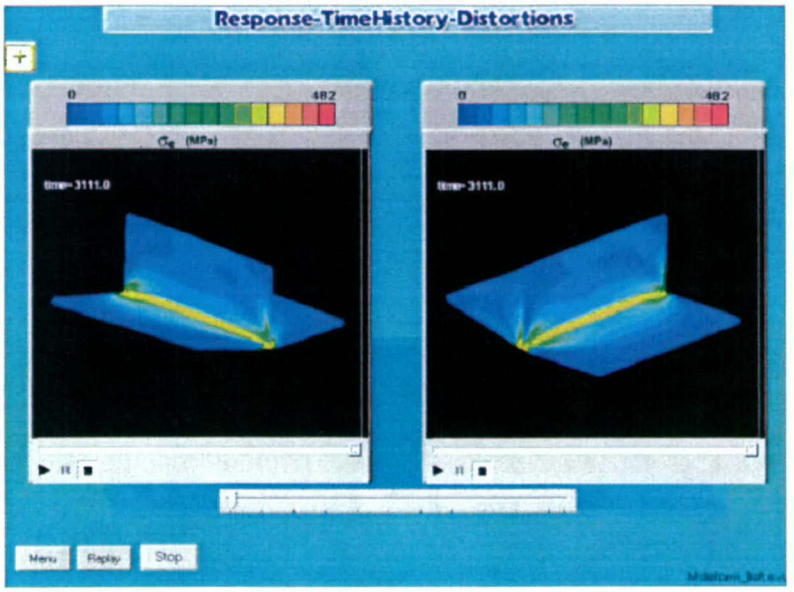
Response-TimeHistory-Distortions
0
482
(MPa)
time=3111.0
0
482
(MPa)
time=3111.0
Menu
Replay
Stop

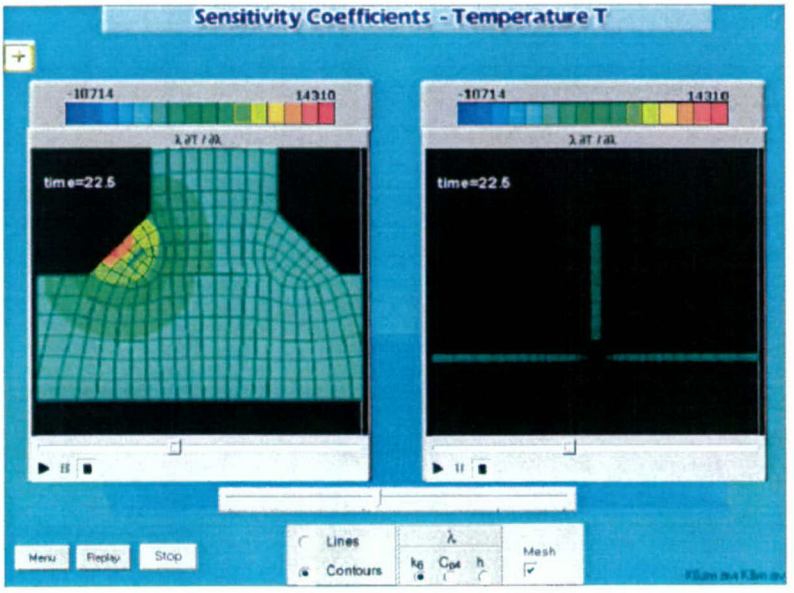
Sensitivity Coefficients - Temperature T
-10714
14310
time=22.5
-10714
14310
time=22.5
Menu
Replay
Stop
Lines
Contours
Mesh

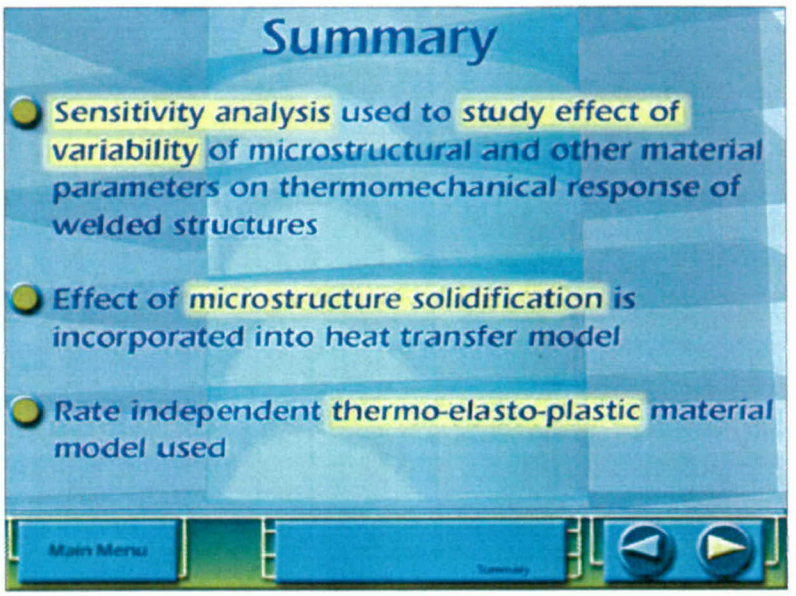
Summary
Sensitivity analysis used to study effect of variability of microstructural and other material parameters on thermomechanical response of welded structures
Effect of microstructure solidification is incorporated into heat transfer model
Rate independent thermo-elasto-plastic material model used
Main Menu

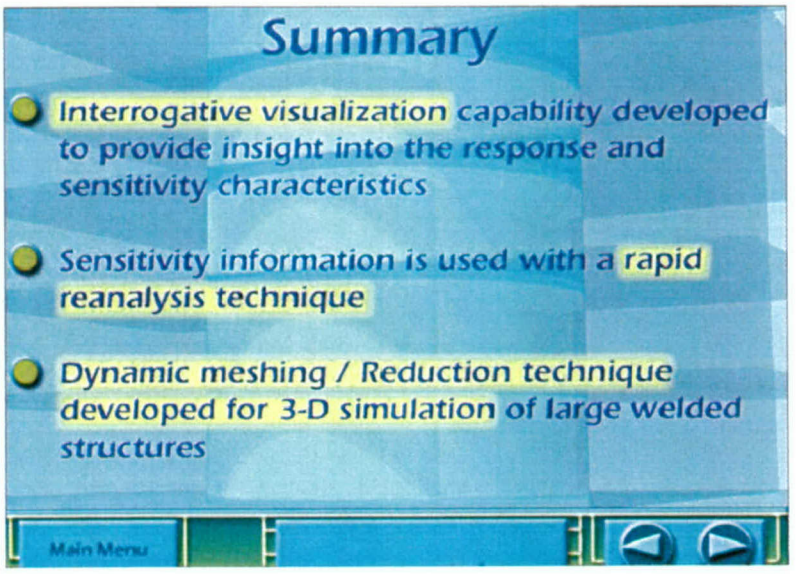
Summary
Interrogative visualization capability developed to provide insight into the response and sensitivity characteristics
Sensitivity information is used with a rapid reanalysis technique
Dynamic meshing / Reduction technique developed for 3-D simulation of large welded structures
Main Menu

Future Work

- Assess the reliability of the materials models incorporating microscopic solidification and metallurgical transformation (with Oak Ridge, Lehigh University and Penn State teams)
  - Systematic verification, validation and calibration of models
- Explore processing methods for reducing residual stresses and distortions in stainless steel ADH fabrication (with Oak Ridge, Lehigh University, Penn State, and Navy Lab teams)
  - Effective use of sensitivity information

Main Menu

Future Work

- Apply the methodologies developed to large welded structures (with Oak Ridge, Navy Lab and other teams)

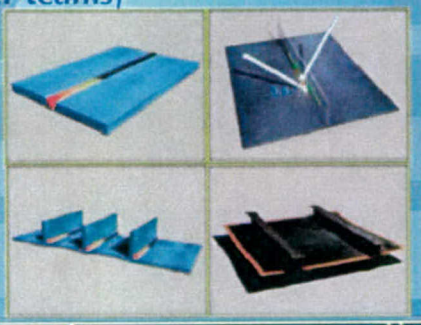

Main Menu